

A window on the CP-violating phases of MSSM from lepton flavor violating processes

This article has been downloaded from IOPscience. Please scroll down to see the full text article.

JHEP01(2009)022

(<http://iopscience.iop.org/1126-6708/2009/01/022>)

[The Table of Contents](#) and [more related content](#) is available

Download details:

IP Address: 80.92.225.132

The article was downloaded on 03/04/2010 at 11:36

Please note that [terms and conditions apply](#).

A window on the CP-violating phases of MSSM from lepton flavor violating processes

S. Yaser Ayazi and Yasaman Farzan

Institute for Research in Fundamental Sciences (IPM),

P.O. Box 19395-5531, Tehran, Iran

E-mail: yaserayazi@mail.ipm.ir, yasaman@theory.ipm.ac.ir

ABSTRACT: It has recently been shown that by measuring the transverse polarization of the final particles in the LFV processes $\mu \rightarrow e\gamma$, $\mu \rightarrow eee$ and $\mu N \rightarrow eN$, one can derive information on the CP-violating phases of the underlying theory. We derive formulas for the transverse polarization of the final particles in terms of the couplings of the effective potential leading to these processes. We then study the dependence of the polarizations of e and γ in the $\mu \rightarrow e\gamma$ and $\mu N \rightarrow eN$ on the parameters of the Minimal Supersymmetric Standard Model (MSSM). We show that combining the information on various observables in the $\mu \rightarrow e\gamma$ and $\mu N \rightarrow eN$ search experiments with the information on the electric dipole moment of the electron can help us to solve the degeneracies in parameter space and to determine the values of certain phases.

KEYWORDS: Supersymmetry Phenomenology.

Contents

1. Introduction	1
2. Polarization of the final particles	2
3. $\mu - e$ conversion	7
4. Effects of the CP-violating phases of MSSM	8
5. Resolving degeneracies	18
6. Conclusions	20

1. Introduction

In the framework of the Standard Model (SM), Lepton Flavor Violating (LFV) processes such as $\mu^+ \rightarrow e^+\gamma$, $\mu^+ \rightarrow e^+e^-e^+$ and $\mu - e$ conversion on nuclei (i.e., $\mu N \rightarrow eN$) are forbidden. Within the SM augmented with neutrino mass and mixing, such processes are in principle allowed but the rates are suppressed by factors of $(\Delta m_\nu^2/E_W^2)^2$ [1] and are too small to be probed in the foreseeable future.

Various models beyond the SM can give rise to LFV rare decay with branching ratios exceeding the present bounds [2]:

$$\text{Br}(\mu^+ \rightarrow e^+\gamma) < 1.2 \times 10^{-11} \quad \text{Br}(\mu^+ \rightarrow e^+e^+e^-) < 1.0 \times 10^{-12} \quad \text{at 90\% C.L.}$$

For low scale MSSM ($m_{\text{SUSY}} \sim 100$ GeV), these experimental bounds imply stringent bounds on the LFV sources in the Lagrangian. The MEG experiment at PSI [3], which is expected to release data in summer 2009, will eventually be able to probe $\text{Br}(\mu^+ \rightarrow e^+\gamma)$ down to 10^{-13} . In our opinion, it is likely that the first evidence for physics beyond the SM comes from the MEG experiment. If the branching ratio is close to its present bound, the MEG experiment will detect statistically significant number of such events. As a result, making precision measurement will become a possibility within a few years. Muons in the MEG experiment are produced by decay of the stopped pions (at rest) so they are almost 100% polarized. This opens up the possibility of learning about the chiral nature of the underlying theory by studying the angular distribution of the final particles relative to the spin of the parent particle [4]. In ref. [5], it has been shown that by measuring the polarization of the final states in the decay modes $\mu^+ \rightarrow e^+\gamma$ and $\mu^+ \rightarrow e^+e^-e^+$, one can derive information on the CP-violating sources of the underlying theory. Notice that even for the state-of-the-art LHC experiment, it will be quite challenging (if

possible at all) to determine the CP-violating phases in the lepton sector [6]. Suppose the LHC establishes a particular theory beyond the SM such as supersymmetry. In order to learn more about the CP-violating phases, the well-accepted strategy is to build yet a more advanced accelerator such as ILC. Considering the expenses and challenges before constructing such an accelerator, it is worth to give any alternative method such as the one suggested in ref. [5] a thorough consideration. In this paper we elaborate more on this method within the framework of R-parity conserving MSSM.

LFV sources in the Lagrangian can also give rise to sizeable $\mu - e$ conversion rate. There are strong bounds on the rates of such processes [7, 4, 8]:

$$R(\mu\text{Ti} \rightarrow e\text{Ti}) \equiv \frac{\Gamma(\mu\text{Ti} \rightarrow e\text{Ti})}{\Gamma(\mu\text{Ti} \rightarrow \text{capture})} < 6.1 \times 10^{-13} \quad . \quad (1.1)$$

The upper bound on R restricts the LFV sources however, for the time being, the bound from $\mu \rightarrow e\gamma$ is more stringent. The PRISM/PRIME experiment is going to perform a new search for the $\mu - e$ conversion [9]. In case that the values of LFV parameters are close to the present upper bound, a significantly large number of the $\mu - e$ conversion events can be recorded by PRISM/PRIME. Recently it is shown in [10] that if the initial muon is polarized (at least partially), studying the transverse polarization of the electron yields information on the CP-violating phase. In this paper, we elaborate more on this possibility taking into account all the relevant effects in the context of R-parity conserving MSSM.

In the end of the paper, we study the possibility of eliminating the degeneracies of the parameter space by combining information from $\mu \rightarrow e\gamma$ and $\mu - e$ conversion experiments. We then demonstrate that the forthcoming results from d_e search can help us to eliminate the degeneracies further (cf. figures 8a,8b).

The paper is organized as follows: In section 2, using the results of ref. [5], we calculate the polarization of the final particles in decay $\mu \rightarrow e\gamma$ in terms of the couplings of the low energy effective Lagrangian (after integrating out the supersymmetric states). We also briefly discuss $\mu \rightarrow eee$ and the challenges of deriving the CP-violating phases by its study. In section 3, we calculate the transverse polarization of the muon in the $\mu - e$ conversion experiment in terms of the couplings in the effective Lagrangian which give the dominant contribution to $\mu N \rightarrow eN$ within the MSSM. In section 4, we study the overall pattern of the variation of $\langle s_{T_2} \rangle$ and $\langle P_{T_1} s_{T_2} \rangle$ with phases and discuss the regions of the parameter space where the sensitivity to the phases are sizeable. In section 5, we discuss how by combining information from the $\mu \rightarrow e\gamma$ and $\mu N \rightarrow eN$ experiments, we can solve the degeneracies in the parameter space. The conclusions are summarized in section 6.

2. Polarization of the final particles

The low energy effective Lagrangian that gives rise to $\mu \rightarrow e\gamma$ can be written as

$$\mathcal{L} = \frac{A_R}{m_\mu} \bar{\mu}_R \sigma^{\mu\nu} e_L F_{\mu\nu} + \frac{A_L}{m_\mu} \bar{\mu}_L \sigma^{\mu\nu} e_R F_{\mu\nu} + \frac{A_R^*}{m_\mu} \bar{e}_L \sigma^{\mu\nu} \mu_R F_{\mu\nu} + \frac{A_L^*}{m_\mu} \bar{e}_R \sigma^{\mu\nu} \mu_L F_{\mu\nu} \quad , \quad (2.1)$$

where $\sigma^{\mu\nu} = \frac{i}{2}[\gamma^\mu, \gamma^\nu]$ and $F_{\mu\nu}$ is the photon field strength: $F_{\mu\nu} = \partial_\mu \varepsilon_\nu - \partial_\nu \varepsilon_\mu$. A_L and A_R receive contributions from the LFV parameters of MSSM at one loop level [11, 12, 4].

In this section we derive the polarizations of the final particles in the LFV rare decays in terms of A_L and A_R . Let us define the longitudinal and transverse directions as follows: $\hat{l} \equiv \vec{p}_{e^+}/|\vec{p}_{e^+}|$, $\hat{T}_2 \equiv \vec{p}_{e^+} \times \vec{s}_\mu/|\vec{p}_{e^+} \times \vec{s}_\mu|$ and $\hat{T}_1 \equiv \hat{T}_2 \times \hat{l}$. As shown in [5], the partial decay rate of an anti-muon at rest into a positron and a photon with definite spins of \vec{s}_e and \vec{s}_γ is

$$\frac{d\Gamma[\mu^+(P_{\mu^+}) \rightarrow e^+(P_{e^+}, \vec{s}_{e^+})\gamma(P_\gamma, \vec{s}_\gamma)]}{d\cos\theta} = \frac{m_\mu}{8\pi} \left[|\alpha_+|^2 |A_L|^2 (1 + \mathbb{P}_\mu \cos\theta) \sin^2 \frac{\theta_s}{2} \right. \tag{2.2}$$

$$+ |\alpha_-|^2 |A_R|^2 (1 - \mathbb{P}_\mu \cos\theta) \cos^2 \frac{\theta_s}{2}$$

$$\left. - \mathbb{P}_\mu \text{Re}[\alpha_+ \alpha_-^* A_L^* A_R e^{i\phi_s}] \sin\theta \sin\theta_s \right],$$

where \mathbb{P}_μ is the polarization of the anti-muon, θ is the angle between the directions of the spin of the anti-muon and the momentum of the positron, and θ_s is the angle between the spin of the positron and its momentum. In the above formula, ϕ_s is the azimuthal angle that the spin of the final positron makes with the plane of spin of the muon and the momentum of the positron. Finally, α_+ and α_- give the polarization of the final photon:

$$\vec{\varepsilon} \cdot \hat{T}_1 \equiv \sum_{j \in \{1,2,3\}} (\hat{T}_1)_j \varepsilon_j = \frac{\alpha_+ + \alpha_-}{\sqrt{2}} \quad \text{and} \quad \vec{\varepsilon} \cdot \hat{T}_2 \equiv \sum_{j \in \{1,2,3\}} (\hat{T}_2)_j \varepsilon_j = \frac{\alpha_+ - \alpha_-}{\sqrt{2}} i$$

where $\sqrt{|\alpha_+|^2 + |\alpha_-|^2} = 1$. Notice that for a given polarization of the positron, the photon has a definite polarization: i.e., setting $\mathbb{P}_\mu = 100\%$ and $\alpha_+ = \alpha_- e^{-i\phi_s} (A_R^*/A_L^*) \tan\theta/2 \cot\theta_s/2$, we find $d\Gamma/d\cos\theta = 0$. Consider the case that $\mathbb{P}_\mu = 100\%$ and the positron is emitted in the direction of the spin of the muon; i.e., $\theta = 0$. From (2.2), we find that for $\theta_s = \pi$ and $\alpha_+ = 1$, $d\Gamma/d\cos\theta$ is maximal. In other words, in this case, the spins of the positron and the photon are respectively aligned in the direction anti-parallel and parallel to the spin of the muon. This is expected because when $\theta = 0$ there is a cylindrical symmetry around the axis parallel to the spin of the muon and therefore the total angular momentum in the direction of the spin does not receive any contribution from the relative angular momentum. This means the sum of spins in the \hat{l} direction has to be conserved which in turn implies that the decay rate is maximal at $\theta_s = \pi$ and $\alpha_+ = 1$. Similar consideration also applies to the case that the positron is emitted antiparallel to the spin of the muon: For $\theta = \pi$, the emission is maximal at $\theta_s = 0$ and $\alpha_- = 1$.

Summing over the polarization of the final particles in eq. (2.2), we obtain

$$\sum_{\vec{s}_\gamma \vec{s}_{e^+}} \frac{d\Gamma[\mu^+(P_{\mu^+}) \rightarrow e^+(P_{e^+}, \vec{s}_{e^+})\gamma(P_\gamma, \vec{s}_\gamma)]}{d\cos\theta} = \frac{m_\mu}{8\pi} [|A_L|^2 (1 + \mathbb{P}_\mu \cos\theta) + |A_R|^2 (1 - \mathbb{P}_\mu \cos\theta)].$$

Thus, $\Gamma(\mu \rightarrow e\gamma)$ is given by $(|A_L|^2 + |A_R|^2)$. It is convenient to define

$$R_1 \equiv \frac{|A_L|^2 - |A_R|^2}{|A_L|^2 + |A_R|^2}. \tag{2.3}$$

By measuring the total decay rate and the angular distribution of the final particles, one can derive absolute values A_L and A_R . To measure the relative phase of these couplings, the polarization of the final particles also have to be measured.

Let us define the polarizations of the electron and photon in an arbitrary direction \hat{T} respectively as

$$\langle s_T \rangle \equiv \frac{\sum_{\vec{s}_\gamma} \left[d\Gamma \left[\mu^+ \rightarrow e^+(\vec{s}_{e^+} = \frac{1}{2}\hat{T})\gamma(\vec{s}_\gamma) \right] - d\Gamma \left[\mu^+ \rightarrow e^+(\vec{s}_{e^+} = -\frac{1}{2}\hat{T})\gamma(\vec{s}_\gamma) \right] \right]}{\sum_{\vec{s}_\gamma \vec{s}_{e^+}} d\Gamma \left[\mu^+ \rightarrow e^+(\vec{s}_{e^+})\gamma(\vec{s}_\gamma) \right]} \quad (2.4)$$

and

$$\langle P_T \rangle \equiv \frac{\sum_{\vec{s}_{e^+}} d\Gamma \left[\mu^+ \rightarrow e^+(\vec{s}_{e^+})\gamma(\vec{\varepsilon} \parallel \hat{T}) \right]}{\sum_{\vec{s}_\gamma \vec{s}_{e^+}} d\Gamma \left[\mu^+ \rightarrow e^+(\vec{s}_{e^+})\gamma(\vec{s}_\gamma) \right]} \quad (2.5)$$

where $\vec{\varepsilon}$ is the polarization vector of the photon.

From eq. (2.2), we find that the polarization of positron (once we average over the polarizations of the photon) is

$$\langle s_{T_1} \rangle = \langle s_{T_2} \rangle = 0, \quad \langle s_l \rangle = \frac{|A_R|^2(1 - \mathbb{P}_\mu \cos \theta) - |A_L|^2(1 + \mathbb{P}_\mu \cos \theta)}{|A_R|^2(1 - \mathbb{P}_\mu \cos \theta) + |A_L|^2(1 + \mathbb{P}_\mu \cos \theta)}.$$

That is while the linear polarization of the photon (once we sum over the polarization of the positron) is

$$\langle P_{T_1} \rangle = \langle P_{T_2} \rangle = \frac{1}{2}.$$

Unfortunately, neither the polarization of the positron nor the polarization of the photon carries any information on the relative phase of A_L and A_R . However, the double correlation of the polarization carries such information. Let us define double correlation as follows

$$\langle P_{T' S_T} \rangle \equiv \frac{d\Gamma \left[\mu^+ \rightarrow e^+(\vec{s}_{e^+} = \frac{1}{2}\hat{T})\gamma(\vec{\varepsilon} \parallel \hat{T}') \right] - d\Gamma \left[\mu^+ \rightarrow e^+(\vec{s}_{e^+} = -\frac{1}{2}\hat{T})\gamma(\vec{\varepsilon} \parallel \hat{T}') \right]}{\sum_{\vec{s}_\gamma \vec{s}_{e^+}} d\Gamma \left[\mu^+ \rightarrow e^+(\vec{s}_{e^+})\gamma(\vec{s}_\gamma) \right]} \quad (2.6)$$

where \hat{T} and \hat{T}' are arbitrary directions. From eq. (2.2), we find

$$\langle P_{T_1 S_{T_1}} \rangle = -\langle P_{T_2 S_{T_1}} \rangle = \frac{-\mathbb{P}_\mu \text{Re}[A_L^* A_R] \sin \theta}{|A_R|^2(1 - \mathbb{P}_\mu \cos \theta) + |A_L|^2(1 + \mathbb{P}_\mu \cos \theta)} \quad (2.7)$$

and

$$\langle P_{T_1 S_{T_2}} \rangle = -\langle P_{T_2 S_{T_2}} \rangle = \frac{\mathbb{P}_\mu \text{Im}[A_L^* A_R] \sin \theta}{|A_R|^2(1 - \mathbb{P}_\mu \cos \theta) + |A_L|^2(1 + \mathbb{P}_\mu \cos \theta)}. \quad (2.8)$$

Thus, as pointed out in [5], to extract the CP-violating phases both polarization and their correlation have to be measured. Eq. (2.7) gives the correlation of the polarizations for particles emitted along the direction described by θ . Averaging over θ , we find

$$\begin{aligned} \overline{\langle P_{T_1 S_{T_1}} \rangle} &= -\overline{\langle P_{T_2 S_{T_1}} \rangle} = \frac{\int_{-1}^1 \mathbb{P}_\mu \text{Re}[A_L^* A_R] \sin \theta d \cos \theta}{\int_{-1}^1 [|A_R|^2(1 - \mathbb{P}_\mu \cos \theta) + |A_L|^2(1 + \mathbb{P}_\mu \cos \theta)] d \cos \theta} \\ &= \frac{-\pi \mathbb{P}_\mu \text{Re}[A_L^* A_R]}{4(|A_L|^2 + |A_R|^2)} \end{aligned} \quad (2.9)$$

and

$$\begin{aligned} \overline{\langle P_{T_1} s_{T_2} \rangle} &= -\overline{\langle P_{T_2} s_{T_2} \rangle} = \frac{\int_{-1}^1 \mathbb{P}_\mu \text{Im}[A_L^* A_R] \sin \theta d \cos \theta}{\int_{-1}^1 [|A_R|^2 (1 - \mathbb{P}_\mu \cos \theta) + |A_L|^2 (1 + \mathbb{P}_\mu \cos \theta)] d \cos \theta} \\ &= \frac{\pi \mathbb{P}_\mu \text{Im}[A_L^* A_R]}{4(|A_L|^2 + |A_R|^2)}. \end{aligned} \quad (2.10)$$

Notice that to take average over angles, one should weigh the polarization of positron emitted within a given interval $(\theta, \theta + d\theta)$ with the number of emission in this interval and then integrate over angles. That is why we have integrated over $d \cos \theta$ in both the numerator and denominator of the right-hand side of the ratios in eqs. (2.7,2.8) instead of calculating $\int \langle P_{T_i} s_{T_j} \rangle d \cos \theta / \int d \cos \theta$.

From eqs. (2.7), (2.8), we find that if the polarimeter is located at $\theta = \pi/2$, the polarization and therefore sensitivity is maximal. Notice that

$$\langle P_{T_i} s_{T_j} \rangle |_{\theta=\pi/2} = \frac{4}{\pi} \overline{\langle P_{T_i} s_{T_j} \rangle}.$$

Measurement of $\overline{\langle P_{T_i} s_{T_j} \rangle}$ requires setting polarimeters all around the region where the decay takes place. In section 4, we perform an analysis of $\overline{\langle P_{T_i} s_{T_j} \rangle}$. Up to a factor of $4/\pi$, our results applies to the case that measurement of the polarization is performed only at $\theta = \pi/2$.

The ratios of the polarizations yield the relative phase of the effective couplings

$$\frac{\langle P_{T_1} s_{T_2} \rangle}{\langle P_{T_1} s_{T_1} \rangle} = \frac{\overline{\langle P_{T_1} s_{T_2} \rangle}}{\overline{\langle P_{T_1} s_{T_1} \rangle}} = \frac{\langle P_{T_2} s_{T_2} \rangle}{\langle P_{T_2} s_{T_1} \rangle} = \frac{\overline{\langle P_{T_2} s_{T_2} \rangle}}{\overline{\langle P_{T_2} s_{T_1} \rangle}} = -\frac{\text{Im}[A_L^* A_R]}{\text{Re}[A_L^* A_R]}.$$

Techniques for the measurement of the transverse polarization of the positron have already been developed and employed for deriving the Michel parameters [13]. Measuring the linear polarization of the photon is going to be more challenging but is in principle possible [14].

In the following, we discuss the LFV process $\mu^+ \rightarrow e^+ e^- e^+$. The effective Lagrangian shown in eq. 2.1 can also give rise to LFV rare decay $\mu^+ \rightarrow e^+ e^- e^+$ through penguin diagrams. Moreover, the process can also receive contributions from the LFV four-fermion terms of the form

$$C_i \bar{\mu} \Gamma_i^\mu (a_i P_L + b_i P_R) e \bar{e} \Gamma_{i,\mu} (c_i P_L + d_i P_R) e$$

where a_i, b_i, c_i and d_i are numbers of order one and $\Gamma_{i,\mu} = \gamma_\mu$ or 1. In the framework of R-parity conserving MSSM which is the focus of the present study, the couplings of the four-fermion interaction are suppressed; i.e., $m_\mu^2 C_i \ll A_{L,R}$. Moreover, the contributions of the A_L and A_R terms for the case that the momentum of one of the positrons is close to $m_\mu/2$ is dramatically enhanced because in this limit the virtual photon in the corresponding diagram goes on-shell. In [5], it is shown that by studying the transverse polarization of the positron whose energy is close to $m_\mu/2$, one can extract information on the phases of the underlying theory. The maximum energy of the positrons emitted in the decay $\mu^+ \rightarrow e^+ e^- e^+$ is $E_{\text{max}} \simeq m_\mu/2 - 3m_e^2/(2m_\mu)$. Consider the case that one of the positrons,

e_1^+ , has an energy close to E_{\max} ; i.e., $E_{\max} - \Delta E < E_1 < E_{\max}$ where $\Delta E \ll m_\mu$. Following [5], let us define

$$\frac{d\Gamma^{\text{Max}}}{d \cos \theta d\phi} = \sum_{s_{e_2^+}, s_{e^-}} \int_{E_{\max} - \Delta E}^{E_{\max}} \int \frac{d\Gamma(\mu^+ \rightarrow e_1^+ e^- e_2^+)}{dE_2 dE_1 d \cos \theta d\phi} dE_2 dE_1, \quad (2.11)$$

where θ is the angle between the spin of the muon and the momentum of e_1^+ (the positron whose energy is close to E_{\max}) and ϕ is the azimuthal angle that the momentum of e_2^+ makes with the plane made by the momentum of e_1^+ and the spin of the muon. Let us suppose that a cut is employed that picks up only events with E_1 within $(E_{\max}, E_{\max} - \Delta E)$ where $2m_e < \Delta E \ll m_\mu$. Because of the enhancement of the amplitude at $E_1 \rightarrow E_{\max}$, the number of events passing the cut is still significant: i.e., $\Gamma^{\text{Max}}/\Gamma_{\text{tot}}(\mu^+ \rightarrow e^+ e^- e^+) = \log(m_\mu \Delta E / 4m_e^2) / (\log(m_\mu^2 / 4m_e^2) - 7/12) > 50\%$. As shown in [5],

$$\begin{aligned} \frac{d\Gamma^{\text{Max}}}{d \cos \theta d\phi} &= \frac{\alpha m_\mu}{192\pi^3} [|A_L|^2 |c_e|^2 (1 + \mathbb{P}_\mu \cos \theta) + |A_R|^2 |d_e|^2 (1 - \mathbb{P}_\mu \cos \theta) \\ &\quad + \mathbb{P}_\mu \sin \theta (\cos(2\phi) \text{Re}[A_R A_L^* d_e c_e^*] + \sin(2\phi) \text{Im}[A_R A_L^* d_e c_e^*])] \log \frac{m_\mu \Delta E}{4m_e^2}, \end{aligned} \quad (2.12)$$

where \mathbb{P}_μ is the polarization of the initial muon and c_e and d_e are the elements of the spinor of e_1^+ : $v_{e_1^+} = \sqrt{2E_1}(0, d_e, c_e, 0)^T$ where $(|d_e|^2 + |c_e|^2)^{1/2} = 1$ and the z -direction is taken to be along the momentum of e_1^+ . Using the above formula it is straightforward to show that the transverse polarization of e_1^+ is

$$\langle s_{T_1} \rangle = \frac{\mathbb{P}_\mu \sin \theta (\cos 2\phi \text{Re}[A_R A_L^*] + \sin 2\phi \text{Im}[A_R A_L^*])}{|A_L|^2 (1 + \mathbb{P}_\mu \cos \theta) + |A_R|^2 (1 - \mathbb{P}_\mu \cos \theta)}$$

and

$$\langle s_{T_2} \rangle = \frac{\mathbb{P}_\mu \sin \theta (-\cos 2\phi \text{Im}[A_R A_L^*] + \sin 2\phi \text{Re}[A_R A_L^*])}{|A_L|^2 (1 + \mathbb{P}_\mu \cos \theta) + |A_R|^2 (1 - \mathbb{P}_\mu \cos \theta)},$$

where $\hat{T}_2 = -(\vec{s}_\mu \times \vec{p}_{e_1^+})/|\vec{s}_\mu \times \vec{p}_{e_1^+}|$ and $\hat{T}_1 = (\hat{T}_2 \times \vec{p}_{e_1^+})/|\hat{T}_2 \times \vec{p}_{e_1^+}|$.

Notice that the averages of $\langle s_{T_1} \rangle$ and $\langle s_{T_2} \rangle$ over ϕ vanish, so to extract information on $\arg[A_R A_L^*]$, one has to measure the azimuthal angle that the momentum of the second positron makes with the plane made by \vec{s}_μ and $\vec{p}_{e_1^+}$. However, measuring ϕ will be challenging because when $(P_\mu - P_{e_1^+})^2 \rightarrow 0$, the angle between the momenta of the two emitted positrons converges to π . For general configuration with $(P_\mu - P_{e_{1,2}^+})^2 \sim m_\mu^2$, the transverse polarization of the electron also carries information on the CP-violating phases of the underlying theory. In the framework we are studying (R-parity conserved MSSM), the rate of $\mu^+ \rightarrow e^+ e^- e^+$ is small compared to the rate of $\mu^+ \rightarrow e^+ \gamma$: $\text{Br}(\mu^+ \rightarrow e^+ e^+ e^-) / \text{Br}(\mu^+ \rightarrow e^+ \gamma) \simeq \frac{\alpha}{3\pi} [\log(m_\mu^2 / m_e^2) - 11/4] \simeq 0.0061$. Thus, even if the present bound on $\mu \rightarrow e\gamma$ is saturated, the statistics of $\mu \rightarrow eee$ will be too low to perform such measurements in the foreseeable future. For this reason, in this paper we will not elaborate on $\mu \rightarrow eee$ any further.

3. $\mu - e$ conversion

In the range of parameter space that we are interested in, the dominant contribution to the $\mu - e$ conversion comes from the γ and Z boson exchange penguin diagrams and the effects of four-Fermi LFV terms can be neglected. The effective LFV vertex in the penguin diagrams can be parameterized as follows

$$\begin{aligned} \mathcal{L}_{\text{eff}} = & \frac{e}{\sin \theta_W \cos \theta_W m_Z^2} \sum_{q \in \{u, d\}} (H_L \bar{e}_L \gamma^\mu \mu_L + H_R \bar{e}_R \gamma^\mu \mu_R) (Z_L^q \bar{q}_L \gamma_\mu q_L + Z_R^q \bar{q}_R \gamma_\mu q_R) \\ & - \sum_{q \in \{u, d\}} \frac{Q_q e}{p^2} \left(B_L^* \bar{e}_L \gamma_\mu \mu_L + B_R^* \bar{e}_R \gamma_\mu \mu_R + i \frac{A_R^*}{m_\mu} \bar{e}_L \sigma^{\mu\nu} p_\nu \mu_R \right. \\ & \left. + i \frac{A_L^*}{m_\mu} \bar{e}_R \sigma^{\mu\nu} p_\nu \mu_L \right) (\bar{q} \gamma_\mu q) + \text{H.c.} \end{aligned} \quad (3.1)$$

where $p = p_\mu - p_e$ is the four-momentum transferred by the photon or Z -boson and Q_q is the electric charge of the quark. $Z_{L(R)}^q = T_q^3 - Q_q \sin^2 \theta_W$ is the coupling of left(right)-handed quark to the Z -boson. H_L and H_R are the effective couplings of the Z boson to lepton. A_L and A_R are the same couplings that appear in eq. (2.1). $B_L(p^2)$ and $B_R(p^2)$ vanish for $p^2 \rightarrow 0$ so they do not contribute to $\mu \rightarrow e\gamma$. Let us evaluate and compare the contributions of the various couplings appearing in eq. (3.1). Since A_L and A_R flip the chirality, they are suppressed by a factor of m_μ . Ward identity implies that B_R and B_L are suppressed by $p^2 = -m_\mu^2$. There is not such a suppression in H_L and H_R , thus $H_{L(R)}/m_Z^2 \sim B_{L(R)}/m_\mu^2$.

$$\frac{d\Gamma(\mu N \rightarrow e N)}{d \cos \theta} = S \left[\frac{1 - \mathbb{P}_\mu \cos \theta}{2} |a H_L + b(A_R^* + B_L^*)|^2 + \frac{1 + \mathbb{P}_\mu \cos \theta}{2} |a H_R + b(A_L^* + B_R^*)|^2 \right], \quad (3.2)$$

where S is a numerical factor that includes the nuclear form factor [11] and

$$a = \frac{e [Z(1/2 - 2 \sin^2 \theta_W) - N/2]}{2m_Z^2 \sin \theta_W \cos \theta_W} \quad \text{and} \quad b = \frac{eZ}{m_\mu^2} \quad (3.3)$$

in which Z and N are respectively the numbers of protons and neutrons inside the nucleus.

Let us define

$$K_R \equiv a H_L + b(A_R^* + B_L^*) \quad (3.4)$$

and

$$K_L \equiv a H_R + b(A_L^* + B_R^*). \quad (3.5)$$

From eq. (3.2), we observe that the total conversion rate, $\int (d\Gamma/d \cos \theta) d \cos \theta$ provides us with information on the sum of $|K_R|^2$ and $|K_L|^2$. That is while by studying the angular distribution of the final electron, we can also extract

$$R_2 \equiv \frac{|K_R|^2 - |K_L|^2}{|K_R|^2 + |K_L|^2}. \quad (3.6)$$

Let us now study what extra information can be extracted by measuring the spin of the final electron.

Similarly to the case of $\mu \rightarrow e\gamma$, let us define the directions \hat{T}_1 and \hat{T}_2 as follows: $\hat{T}_2 = (\vec{p}_e \times \vec{s}_\mu)/|\vec{p}_e \times \vec{s}_\mu|$ and $\hat{T}_1 = ((\vec{p}_e \times \vec{s}_\mu) \times \vec{p}_e)/|(\vec{p}_e \times \vec{s}_\mu) \times \vec{p}_e|$. Let us also define

$$\langle s_{T_i} \rangle \equiv \frac{d\Gamma \left[\mu N \rightarrow e(\vec{s}_e = \frac{1}{2}\hat{T}_i)N \right] - d\Gamma \left[\mu N \rightarrow e(\vec{s}_e = -\frac{1}{2}\hat{T}_i)N \right]}{\sum_{\vec{s}_e} d\Gamma[\mu N \rightarrow eN]}.$$

It is straightforward to verify that the transverse polarization of the emitted electron in the directions of \hat{T}_1 and \hat{T}_2 are

$$\langle s_{T_1} \rangle = \frac{2\text{Re}[K_R K_L^*] \mathbb{P}_\mu \sin \theta}{|K_R|^2(1 - \mathbb{P}_\mu \cos \theta) + |K_L|^2(1 + \mathbb{P}_\mu \cos \theta)}, \quad (3.7)$$

$$\langle s_{T_2} \rangle = \frac{2\text{Im}[K_R K_L^*] \mathbb{P}_\mu \sin \theta}{|K_R|^2(1 - \mathbb{P}_\mu \cos \theta) + |K_L|^2(1 + \mathbb{P}_\mu \cos \theta)}. \quad (3.8)$$

Averaging over the angular distribution, we find

$$\overline{\langle s_{T_1} \rangle} \equiv \frac{\int \langle s_{T_1} \rangle \frac{d\Gamma}{d\cos\theta} d\cos\theta}{\int \frac{d\Gamma}{d\cos\theta} d\cos\theta} = \frac{\pi \text{Re}[K_R K_L^*] \mathbb{P}_\mu}{2(|K_R|^2 + |K_L|^2)}, \quad (3.9)$$

and

$$\overline{\langle s_{T_2} \rangle} \equiv \frac{\int \langle s_{T_2} \rangle \frac{d\Gamma}{d\cos\theta} d\cos\theta}{\int \frac{d\Gamma}{d\cos\theta} d\cos\theta} = \frac{\pi \text{Im}[K_R K_L^*] \mathbb{P}_\mu}{2(|K_L|^2 + |K_R|^2)}. \quad (3.10)$$

The advantage of the study of the $\mu - e$ conversion over the study of $\mu \rightarrow e\gamma$ is that in the former case there is no need for performing the challenging photon polarization measurement. The drawback is the polarization of the initial muon. While the polarization of muon in the $\mu \rightarrow e\gamma$ experiments is close to 100%, the muons orbiting the nuclei (the muons in the $\mu - e$ conversion experiments) suffer from low polarization of 16% or lower [15]. However, there are proposals to “re-”polarize the muon in the muonic atoms by using polarized nuclear targets [16].

In this paper, we take $\mathbb{P}_\mu = 20\%$. For any given value of \mathbb{P}_μ , our results can be simply re-scaled.

4. Effects of the CP-violating phases of MSSM

In this section, we study the polarizations introduced in the previous section in the framework of R-parity conserving Minimal Supersymmetric Standard Model (MSSM). The part of the superpotential that is relevant to this study can be written as

$$W_{\text{MSSM}} = -Y_i \widehat{e}_{Ri}^c \widehat{L}_i \cdot \widehat{H}_d - \mu \widehat{H}_u \cdot \widehat{H}_d \quad (4.1)$$

where \widehat{L}_i , \widehat{H}_u and \widehat{H}_d are doublets of chiral superfields associated respectively with the left-handed lepton doublets and the two Higgs doublets of the MSSM. \widehat{e}_{Ri}^c is the chiral superfield associated with the right-handed charged lepton field, e_{Ri}^c . The index “ i ” is the

flavor index. At the electroweak scale, the soft supersymmetry breaking part of Lagrangian in general has the following form

$$\begin{aligned}
 \mathcal{L}_{\text{soft}}^{\text{MSSM}} = & -1/2 \left(M_1 \widetilde{B}\widetilde{B} + M_2 \widetilde{W}\widetilde{W} + \text{H.c.} \right) \\
 & - \left((A_i Y_i \delta_{ij} + A_{ij}) \widetilde{e}_{Ri}^c \widetilde{L}_j \cdot H_d + \text{H.c.} \right) - \widetilde{L}_i^\dagger (m_L^2)_{ij} \widetilde{L}_j - \widetilde{e}_{Ri}^c{}^\dagger (m_R^2)_{ij} \widetilde{e}_{Rj}^c \\
 & - m_{H_u}^2 H_u^\dagger H_u - m_{H_d}^2 H_d^\dagger H_d - (B_H H_u \cdot H_d + \text{H.c.}), \tag{4.2}
 \end{aligned}$$

where the “ i ” and “ j ” indices determine the flavor and \widetilde{L}_i consists of $(\widetilde{\nu}_i \widetilde{e}_{Li})$. Notice that we have divided the trilinear coupling to a diagonal flavor part $(A_i Y_i \delta_{ij})$ and a LFV part $(A_{ij}$ with $A_{ii} = 0)$. Terms involving the squarks as well as the gluino mass term have to be added to eqs. (4.1), (4.2) but these terms are not relevant to this study. The Hermiticity of the Lagrangian implies that $m_{H_u}^2$, $m_{H_d}^2$, and the diagonal elements of m_L^2 and m_R^2 are all real. Moreover, without loss of generality, we can rephase the fields to make the parameters M_2 , B_H as well as Y_i real. In such a basis, the rest of the above parameters can in general be complex and can be considered as sources of CP-violation. After electroweak symmetry breaking, A_{ij} gives rise to LFV masses:

$$(m_{LR}^2)_{ij} = A_{ij} \langle H_d \rangle \quad \text{for } i \neq j.$$

Notice that in general $|A_{ij}| \neq |A_{ji}|$ and therefore $|(m_{LR}^2)_{ij}| \neq |(m_{LR}^2)_{ji}|$.

The CP-violating phases that can in principle show up in the polarizations studied in the previous sections are the phases of A_i , the μ -term, M_1 (the Bino mass) and phases of LFV elements of mass matrices in soft supersymmetry breaking Lagrangian. The strong bound on the electric dipole moment of the electron implies strong bounds on the phases of A_e , μ and M_1 (*see*, however [17]). For this reason, in this paper, we set the phases of these parameters equal to zero and focus on the effects of the phases of A_μ and the LFV elements of mass matrices. In the present analysis, we focus on the effects of the $e\mu$ elements. Effects of $e\tau$ and $\mu\tau$ elements will be explored elsewhere.

Once we turn on the LFV terms, the phase of A_μ as well as the phases of the LFV elements can contribute to d_e at one loop level [18, 19]. We therefore have to make sure that the bounds on d_e are satisfied. For the parameters that we have considered in this analysis, the contributions of the phases of $e\mu$ elements to d_e are of order of $\sim 10^{-29}$ e cm and well below the present bound [2]. The contribution of the phase of A_μ is even lower by one order of magnitude. In the next section, we shall discuss the role of the forthcoming results of d_e searches in reducing the degeneracies.

As the reference point, we have chosen the mass spectra corresponding to the $P3$ benchmark which has been proposed in [20]. We have however let A_e and A_μ deviate from the corresponding values at the benchmark $P3$. The values of A_i and A_{ij} are chosen such that they satisfy the constraints from Color and Charge Breaking (CCB) as well as Unbounded From Below (UFB) considerations [21]. The rest of the bounds and restrictions on the parameters of supersymmetry are undisturbed by varying A_i .

Figures 1–3 shows R_1 , $\text{Br}(\mu \rightarrow e\gamma)$, $\langle \overline{P_{T_1} s_{T_1}} \rangle$ and $\langle \overline{P_{T_1} s_{T_2}} \rangle$ (*see*, eqs. (2.3), (2.9), (2.10) for definitions) versus the phases of A_μ and the LFV elements. We have set $|A_e| = |A_\mu|$

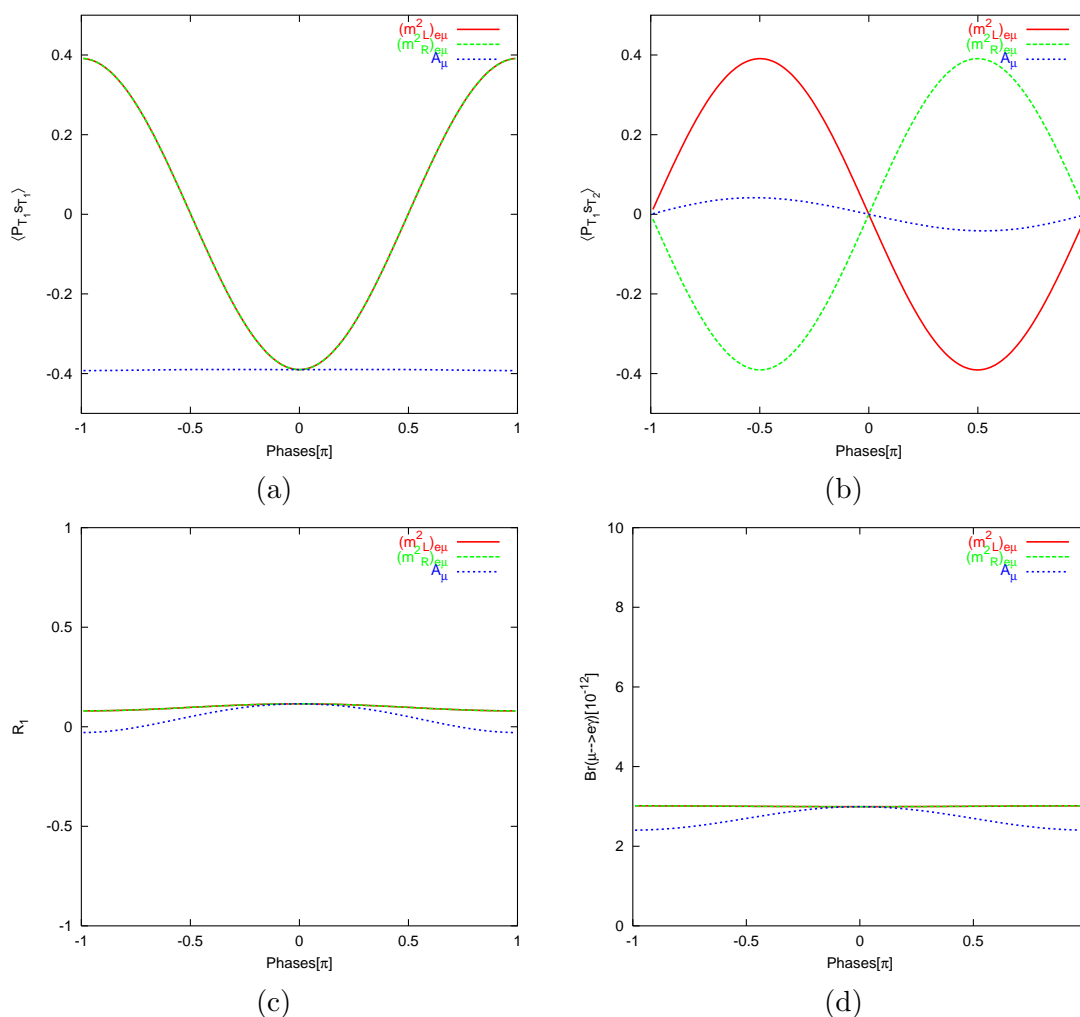


Figure 1: Observable quantities in the $\mu \rightarrow e\gamma$ experiment versus the phases of A_μ , $(m_L^2)_{e\mu}$ and $(m_R^2)_{e\mu}$. The vertical axes in figures (a)–(d) are respectively $\langle P_{T_1} s_{T_1} \rangle$, $\langle P_{T_1} s_{T_2} \rangle$, R_1 and $Br(\mu \rightarrow e\gamma)$. The input parameters correspond to the $P3$ benchmark proposed in [20]: $|\mu| = 400$ GeV, $m_0 = 1000$ GeV, $M_{1/2} = 500$ GeV and $\tan\beta = 10$ and we have set $|A_\mu| = |A_e| = 700$ GeV. All the LFV elements of the slepton mass matrix are set to zero except $(m_L^2)_{e\mu} = 2500$ GeV² and $(m_R^2)_{e\mu} = 12500$ GeV². We have taken $\mathbb{P}_\mu = 100\%$.

however the results are robust against varying the values of $|A_e|$ as expected. In figure 1, we have taken A_{ij} and all the LFV elements of the slepton mass matrix other than $(m_L^2)_{e\mu}$ and $(m_R^2)_{e\mu}$ equal to zero. Notice that $(m_L^2)_{e\mu}$ and $(m_R^2)_{e\mu}$ have been chosen such that $Br(\mu \rightarrow e\gamma)$ lies close to its present experimental upper bound. As seen from figure 1c, for such choice of $(m_L^2)_{e\mu}$ and $(m_R^2)_{e\mu}$, R_1 is close to zero which means $|A_L| \approx |A_R|$. As a result, we expect the transverse polarization to be sizable. Figures 1a,1b demonstrate that this expectation is fulfilled. From figures 1a,1b, we also observe that the sensitivity of the transverse polarization to the phases of $(m_L^2)_{e\mu}$ and $(m_R^2)_{e\mu}$ is significant so by measuring these polarizations with a moderate accuracy one can extract information on these phases.

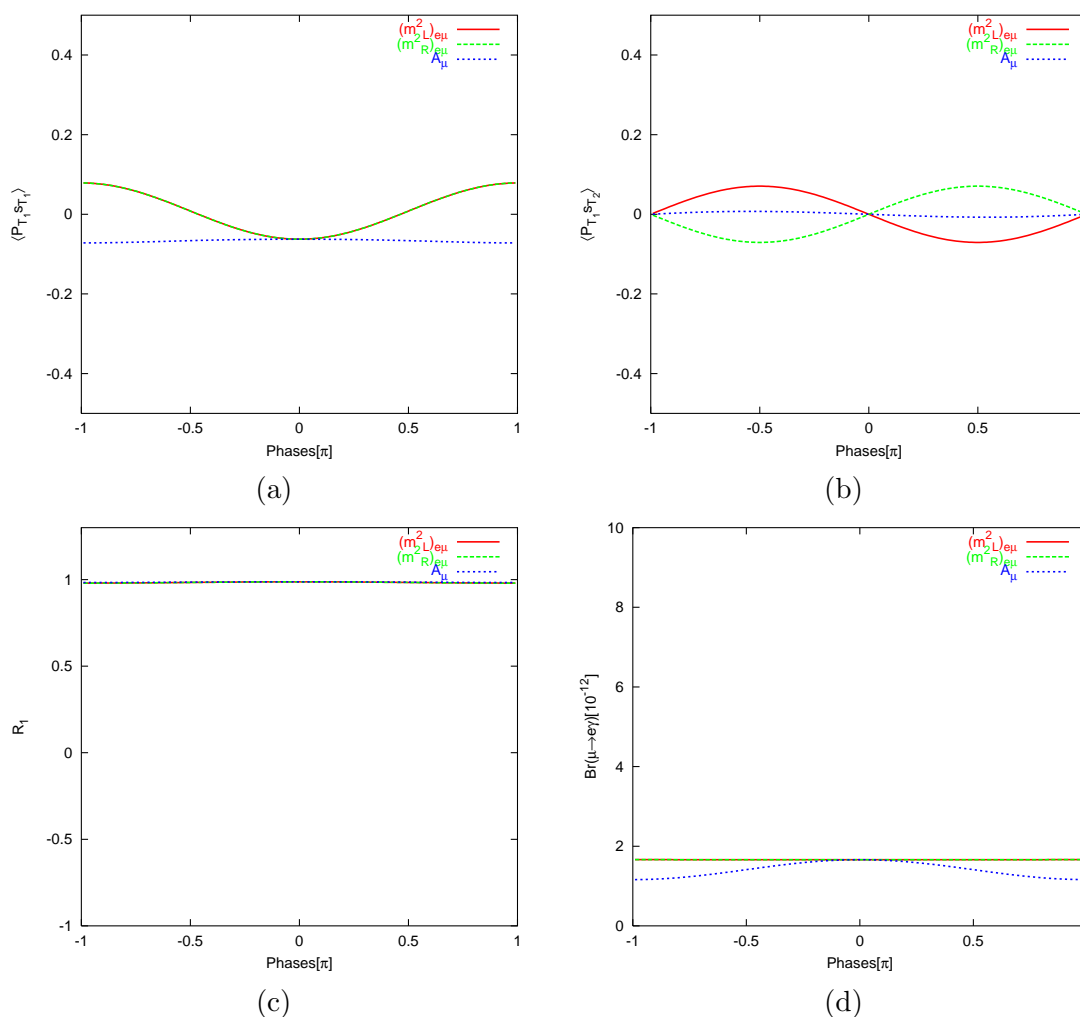


Figure 2: Observable quantities in the $\mu \rightarrow e\gamma$ experiment versus the phases of A_μ , $(m_L^2)_{e\mu}$ and $(m_R^2)_{e\mu}$. The vertical axes in figures (a)–(d) are respectively $\langle P_{T_1} s_{T_1} \rangle$, $\langle P_{T_1} s_{T_2} \rangle$, R_1 and $\text{Br}(\mu \rightarrow e\gamma)$. The input parameters correspond to the $P3$ benchmark proposed in [20]: $|\mu| = 400 \text{ GeV}$, $m_0 = 1000 \text{ GeV}$, $M_{1/2} = 500 \text{ GeV}$ and $\tan\beta = 10$ and we have set $|A_\mu| = |A_e| = 700 \text{ GeV}$. All the LFV elements of the slepton mass matrix are set to zero except $(m_L^2)_{e\mu} = 250 \text{ GeV}^2$ and $(m_R^2)_{e\mu} = 12500 \text{ GeV}^2$. We have taken $\mathbb{P}_\mu = 100\%$.

However at this benchmark, the sensitivity to the phase of A_μ is quite low.

The input of figure 2 is similar to that of figure 1 except that a hierarchy is assumed between the left and right LFV elements: $|(m_L^2)_{e\mu}| \ll |(m_R^2)_{e\mu}|$. As expected in this case, $R_1 \approx 1$ and the transverse polarizations are small. To draw figure 3, we have set the LFV elements of m_L^2 and m_R^2 equal to zero and instead we have set $A_{e\mu}, A_{\mu e} \neq 0$. As seen in figure 3 in this case, the transverse polarizations can be sizeable.

Figures 4–6 show R_2 , $R(\mu + Ti \rightarrow e + Ti)$, $\langle s_{T_1} \rangle$ and $\langle s_{T_2} \rangle$ (see, eqs. (3.6), (3.9), (3.10) for definitions) versus the phases of A_μ and the LFV elements. To draw the figures corresponding to the $\mu - e$ conversion, we have taken $\mathbb{P}_\mu = 20\%$. If the technical difficulties of

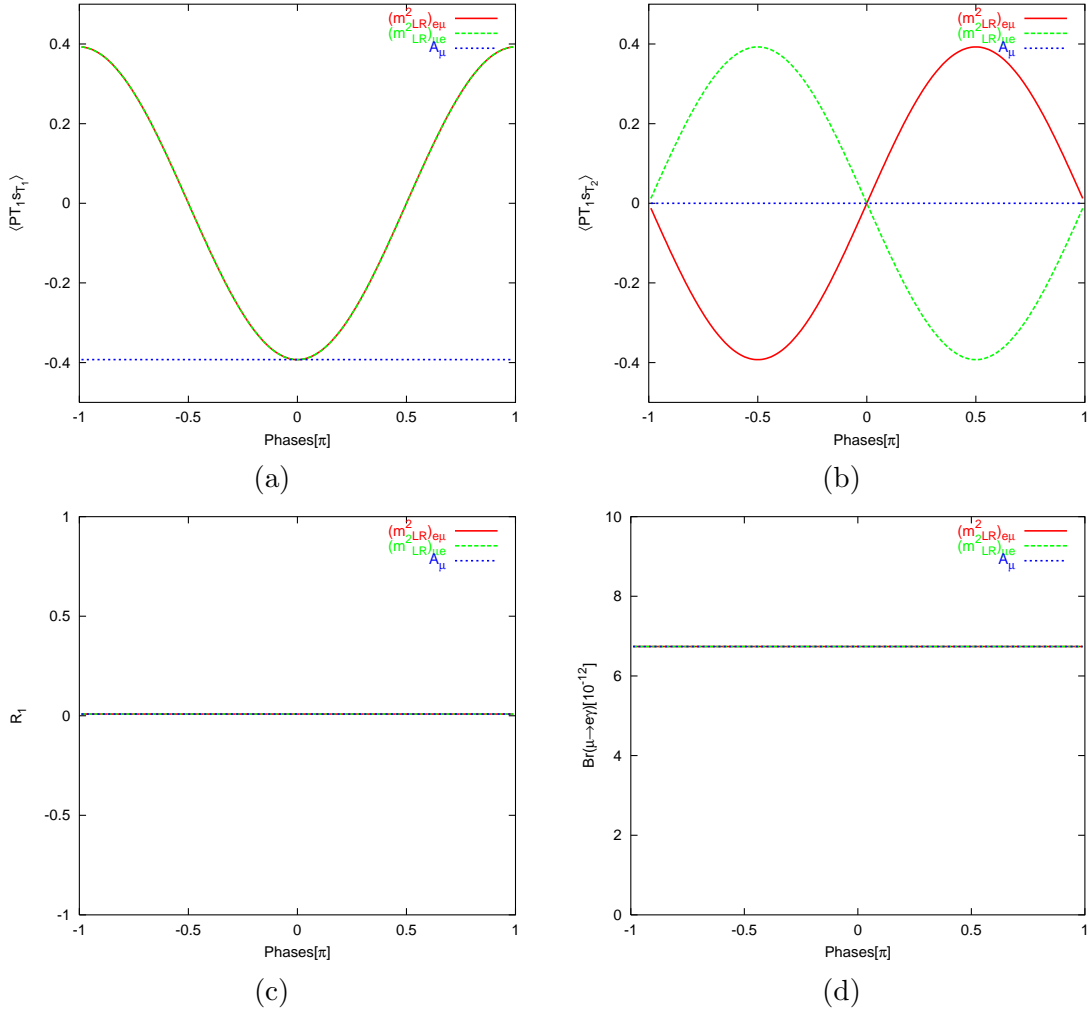


Figure 3: Observable quantities in the $\mu \rightarrow e\gamma$ experiment versus the phases of A_μ , $(m_{LR}^2)_{e\mu}$ and $(m_{LR}^2)_{\mu e}$. The vertical axes in figures (a)–(d) are respectively $\overline{\langle P_{T_1} s_{T_1} \rangle}$, $\overline{\langle P_{T_1} s_{T_2} \rangle}$, R_1 and $\text{Br}(\mu \rightarrow e\gamma)$. The input parameters correspond to the $P3$ benchmark proposed in [20]: $|\mu| = 400 \text{ GeV}$, $m_0 = 1000 \text{ GeV}$, $M_{1/2} = 500 \text{ GeV}$ and $\tan\beta = 10$ and we have set $|A_\mu| = |A_e| = 700 \text{ GeV}$. All the LFV elements of the slepton mass matrix are set to zero except $(m_{LR}^2)_{e\mu} (= A_{e\mu} \langle H_d \rangle) = 14 \text{ GeV}^2$ and $(m_{LR}^2)_{\mu e} (= A_{\mu e} \langle H_d \rangle) = 14 \text{ GeV}^2$. We have taken $\mathbb{P}_\mu = 100\%$.

polarizing the muon in the $\mu - e$ conversion experiment is overcome and higher values of \mathbb{P}_μ is achieved, $\overline{\langle s_{T_1} \rangle}$ and $\overline{\langle s_{T_2} \rangle}$ can become larger. Obviously, for a given value of \mathbb{P}_μ , $\overline{\langle s_{T_1} \rangle}$ and $\overline{\langle s_{T_2} \rangle}$ have to be re-scaled by $(\mathbb{P}_\mu/20\%)$. Apart from the polarization, the input parameters in figures 4,5,6 are respectively the same as the input parameters in figures 1,2,3. Notice that in this case, too, the sensitivity to the phase of A_μ is low. From figure 2, we observe that $\overline{\langle s_{T_2} \rangle}$ increases more rapidly with $\sin[\arg[(m_L^2)_{e\mu}]]$ than with $\sin[\arg[(m_R^2)_{e\mu}]]$. For $|(m_L^2)_{e\mu}| \ll |(m_R^2)_{e\mu}|$ cases, at first sight, higher sensitivity to $\arg[(m_L^2)_{e\mu}]$ may sound counterintuitive. However, notice that as $|\sin[\arg[(m_R^2)_{e\mu}]]|$ increases, R_2 rapidly converges to one which means $K_R \gg K_L$ and therefore $\langle s_{T_2} \rangle \propto \text{Im}[K_R K_L^*] / (|K_L|^2 + |K_R|^2) \rightarrow 0$.

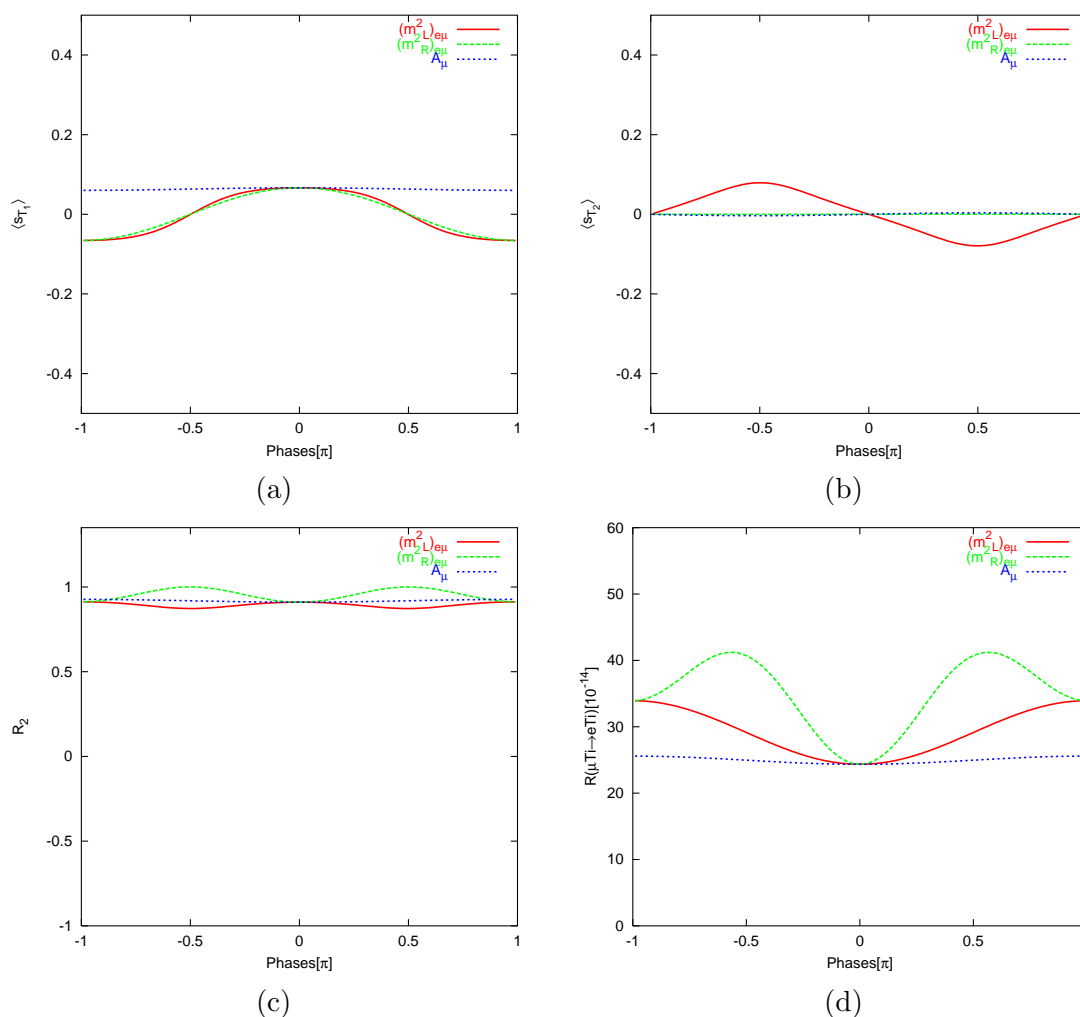


Figure 4: Observable quantities in the $\mu - e$ conversion experiment versus the phases of A_μ , $(m_L^2)_{e\mu}$ and $(m_R^2)_{e\mu}$. The vertical axes in figures (a)–(d) are respectively $\langle s_{T_1} \rangle$, $\langle s_{T_2} \rangle$, R_2 and $R(\mu Ti \rightarrow e Ti)$. The input parameters correspond to the $P3$ benchmark proposed in [20]: $|\mu| = 400$ GeV, $m_0 = 1000$ GeV, $M_{1/2} = 500$ GeV and $\tan \beta = 10$ and we have set $|A_\mu| = |A_e| = 700$ GeV. All the LFV elements of the slepton mass matrix are set to zero except $(m_L^2)_{e\mu} = 2500$ GeV² and $(m_R^2)_{e\mu} = 12500$ GeV². We have taken $\mathbb{P}_\mu = 20\%$.

It is remarkable that in the case of figure 4 for which $(m_L^2)_{e\mu} \sim (m_R^2)_{e\mu}$, R_2 is close to one and the transverse polarizations is relatively small but in the case of figure 5 for which $(m_R^2)_{e\mu} = 50(m_L^2)_{e\mu}$, ($|1 - |R_2|| \sim 1$) and the transverse polarizations become sizeable. We have explored higher hierarchy between the left and right LFV elements and have found that for $(m_L^2)_{e\mu} \lesssim 500(m_R^2)_{e\mu}$, $\langle s_{T_1} \rangle$ and $\langle s_{T_2} \rangle$ diminish. Contrasting figures 4,5 with figures 1,2, we find that the polarization studies at the $\mu \rightarrow e\gamma$ and $\mu - e$ conversion experiments can be complementary. That is if $1 - |R_1| \sim \text{few} \times 0.01$, transverse polarization in the $\mu \rightarrow e\gamma$ will become small making the derivation of the CP-violating phases more challenging. However there is still the hope to derive the phases by polarization studies

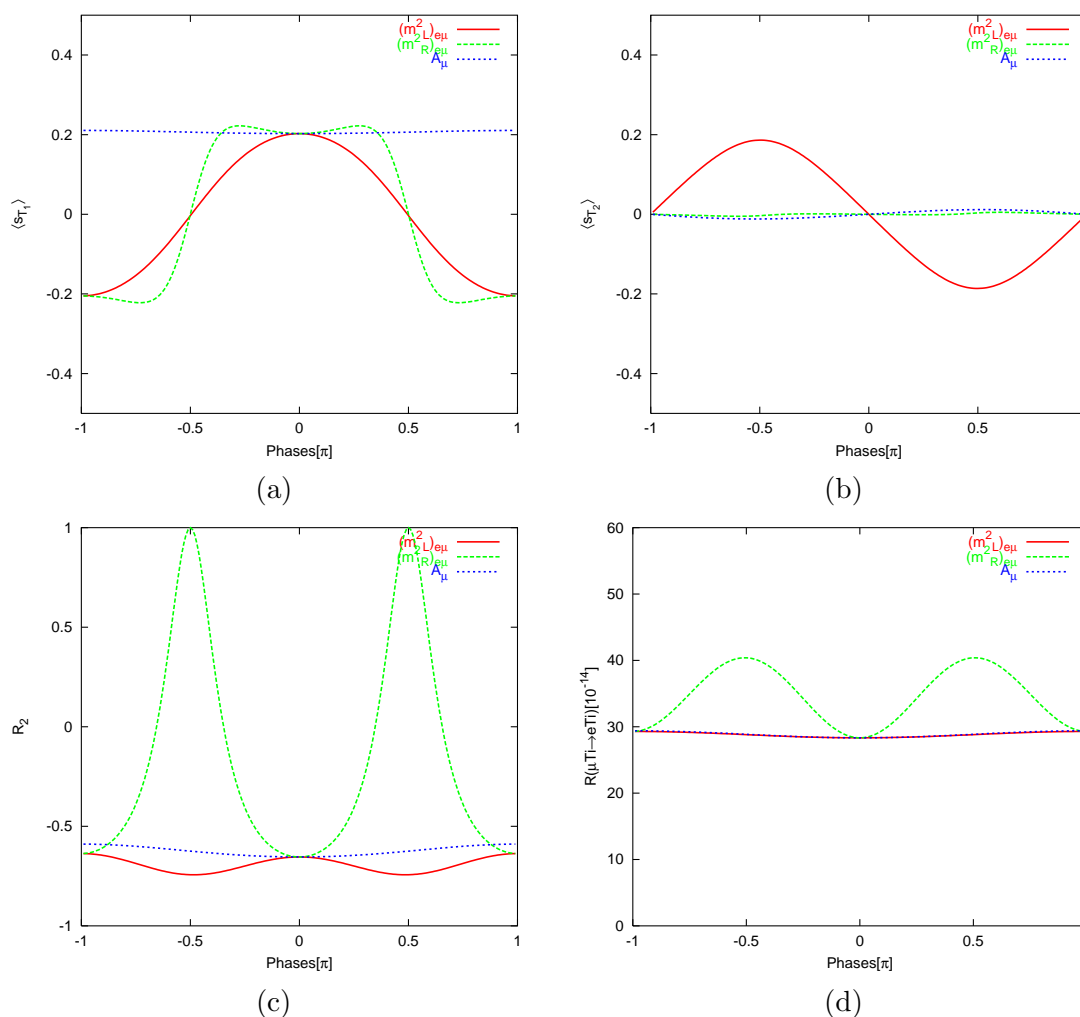


Figure 5: Observable quantities in the $\mu - e$ conversion experiment versus the phases of A_μ , $(m_L^2)_{e\mu}$ and $(m_R^2)_{e\mu}$. The vertical axes in figures (a)–(d) are respectively $\langle s_{T_1} \rangle$, $\langle s_{T_2} \rangle$, R_2 and $R(\mu Ti \rightarrow e Ti)$. The input parameters correspond to the P_3 benchmark proposed in [20]: $|\mu| = 400$ GeV, $m_0 = 1000$ GeV, $M_{1/2} = 500$ GeV and $\tan \beta = 10$ and we have set $|A_\mu| = |A_e| = 700$ GeV. All the LFV elements of the slepton mass matrix are set to zero except $(m_L^2)_{e\mu} = 250$ GeV² and $(m_R^2)_{e\mu} = 12500$ GeV². We have taken $\mathbb{P}_\mu = 20\%$.

at the $\mu - e$ conversion experiments. We shall discuss this point in more detail in the description of figure 7.

Notice that in figures 1–6, which all correspond to the benchmark P_3 , sensitivity to the phase of A_μ is low. This is expected because the effect of A_μ is suppressed by $\tan \beta = 10$. We have checked for the robustness of this result and found that for most of the parameter space with large $\tan \beta$, sensitivity to the phase of A_μ is low but there are points at which sensitivity to ϕ_{A_μ} is considerable; e.g., at δ benchmark which has been proposed in [22].

The following remarks are in order:

- In all of these sets of diagrams, maximal $|\langle s_{T_1} \rangle|$ corresponds to $|\langle s_{T_2} \rangle| = 0$ and vice

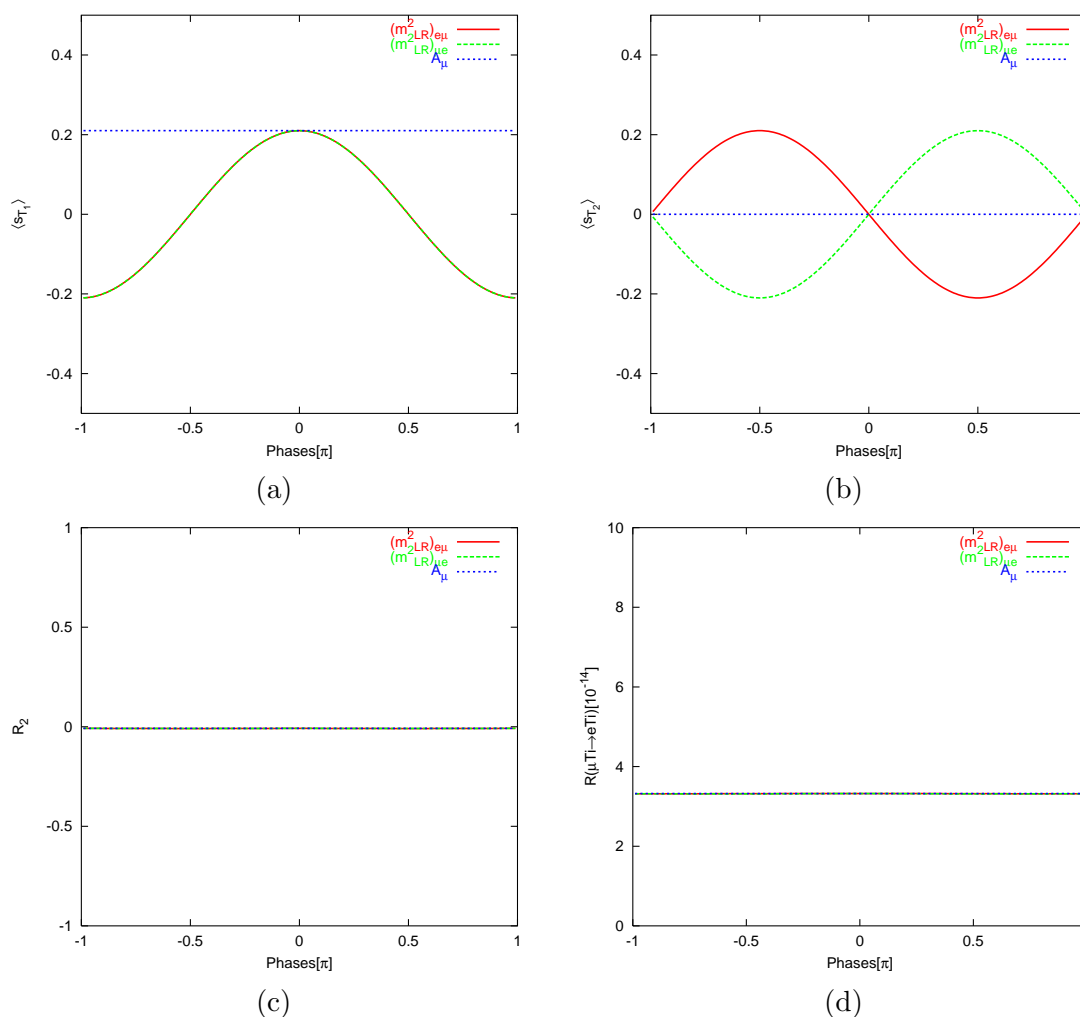


Figure 6: Observable quantities in the $\mu - e$ conversion experiment versus the phases of A_μ , $(m_{LR}^2)_{e\mu}$ and $(m_{LR}^2)_{\mu e}$. The vertical axes in figures (a)–(d) are respectively $\langle s_{T_1} \rangle$, $\langle s_{T_2} \rangle$, R_2 and $R(\mu\text{Ti} \rightarrow e\text{Ti})$. The input parameters correspond to the $P3$ benchmark proposed in [20]: $|\mu| = 400 \text{ GeV}$, $m_0 = 1000 \text{ GeV}$, $M_{1/2} = 500 \text{ GeV}$ and $\tan \beta = 10$ and we have set $A_\mu = A_e = 700 \text{ GeV}$. All the LFV elements of the slepton mass matrix are set to zero except $(m_{LR}^2)_{e\mu} (= A_{e\mu} \langle H_d \rangle) = 14 \text{ GeV}^2$ and $(m_{LR}^2)_{\mu e} (= A_{\mu e} \langle H_d \rangle) = 14 \text{ GeV}^2$. We have taken $\mathbb{P}_\mu = 20\%$.

versa. This is expected from eqs. (3.9) and (3.10) because $\overline{\langle s_{T_1} \rangle}$ and $\overline{\langle s_{T_2} \rangle}$ are respectively given by the real and imaginary parts of the same combinations. For general values of the phases, $|\overline{\langle s_{T_1} \rangle}|^2 + |\overline{\langle s_{T_2} \rangle}|^2$ is solely given by the absolute values of K_L and K_R , and is independent of their relative phase. Remember that $|K_R|$ and $|K_L|$ can be extracted by studying the angular distribution of the electron without measuring its spin. Thus, the simultaneous measurement of R_2 , $\overline{\langle s_{T_1} \rangle}$ and $\overline{\langle s_{T_2} \rangle}$ provides a cross-check. A similar consideration holds for R_1 , $\overline{\langle P_{T_1} s_{T_1} \rangle}$ and $\overline{\langle P_{T_1} s_{T_2} \rangle}$, too.

- When all the phases are set equal to zero, $\langle s_{T_2} \rangle$ and $\langle P_{T_1} s_{T_2} \rangle$ vanish but $\langle s_{T_1} \rangle$ and $\langle P_{T_1} s_{T_1} \rangle$ can be nonzero. Thus, for the purpose of establishing CP, it

will be more convenient to measure $\langle s_{T_2} \rangle$ or $\langle P_{T_1} s_{T_2} \rangle$. This is expected from eqs. (2.9), (2.10), (3.9), (3.10).

- When $(m_{LR}^2)_{e\mu} = (m_{LR}^2)_{\mu e} = 0$, in the case of $\mu \rightarrow e\gamma$, there is a symmetry under $\arg[(m_L^2)_{e\mu}] \leftrightarrow -\arg[(m_R^2)_{e\mu}]$ [see figures 1,2] but in the case of the $\mu - e$ conversion, there is not such a symmetry [see figures 4,5]. Moreover, while the dependence of R_1 on the phases is very mild, R_2 can dramatically change with varying some of the phases (see, e.g., figure 5c). This can be better understood in the limit of the LFV mass insertion approximation. Remember that observables in the $\mu \rightarrow e\gamma$ decay are given by A_L and A_R for $(m_{LR}^2)_{\mu e} = (m_{LR}^2)_{e\mu} = 0$. To leading approximation, A_L and A_R are respectively proportional to $(m_R^2)_{e\mu}$ and $(m_L^2)_{e\mu}$. As a result, when we vary the phase of $(m_R^2)_{e\mu}$, only the phase of A_L changes. Similarly varying $\arg[(m_L^2)_{e\mu}]$ only changes $\arg[A_R]$. Since R_1 depends only on the absolute values of A_R and A_L , it should not change with varying the phases. Remember that $\langle P_{T_1} s_{T_1} \rangle$ and $\langle P_{T_1} s_{T_2} \rangle$ are given by $\text{Re}[A_L A_R^*]$ and $\text{Im}[A_L A_R^*]$ which to leading order are proportional to $\text{Re}[(m_R^2)_{e\mu} (m_L^2)_{e\mu}^*]$ and $\text{Im}[(m_R^2)_{e\mu} (m_L^2)_{e\mu}^*]$. Thus, there should be a symmetry under $\arg[(m_L^2)_{e\mu}] \leftrightarrow -\arg[(m_R^2)_{e\mu}]$ for $(m_{LR}^2)_{\mu e} = (m_{LR}^2)_{e\mu} = 0$. Observables in the $\mu - e$ conversion case depend on K_L and K_R . Unlike A_L and A_R , each of K_L and K_R can receive contributions from both $(m_L^2)_{e\mu}$ and $(m_R^2)_{e\mu}$. Thus, the above argument does not apply here. Similar consideration holds for the case that $(m_{LR}^2)_{\mu e}$ and $(m_{LR}^2)_{e\mu}$ are nonzero but $(m_R^2)_{e\mu} = (m_L^2)_{e\mu} = 0$ (see, figures 3 and 6). As expected, when $(m_R^2)_{e\mu}$, $(m_L^2)_{e\mu}$, $(m_{LR}^2)_{\mu e}$ and $(m_{LR}^2)_{e\mu}$ are all nonzero, the symmetries under $\arg[(m_L^2)_{e\mu}] \leftrightarrow -\arg[(m_R^2)_{e\mu}]$ and $\arg[(m_{LR}^2)_{\mu e}] \leftrightarrow -\arg[(m_{LR}^2)_{e\mu}]$ disappear.
- In this analysis, we have considered the $\mu - e$ conversion only on Titanium. It is possible to perform the experiment on other nuclei such as Au and Al, too. From eqs. (3.2), (3.3), we find that the effects change with changing the nuclei (with change of N and Z). In principle, by studying the conversion rate on different nuclei, one can derive information on different combinations of the phases. However, in practice since the ratio N/Z for different nuclei in question are more or less the same (the difference between N/Z of Au and Al is about 20%), $\langle s_{T_1} \rangle$, $\langle s_{T_2} \rangle$ and R_2 for different nuclei turn out to be close to each other. Only if $\langle s_{T_i} \rangle$ can be measured with accuracy better than 5% (i.e., $\delta\langle s_{T_i} \rangle / \langle s_{T_i} \rangle < 5\%$), using different nuclei will help us to solve degeneracies.

Scatter plots shown in figure 7 demonstrate the configurations of the LFV elements where $\overline{\langle s_{T_2} \rangle}$ or $\overline{\langle P_{T_1} s_{T_2} \rangle}$ can be sizeable. That is where maximal values of $\langle s_{T_2} \rangle$ and $\langle P_{T_1} s_{T_2} \rangle$ are respectively larger than 0.1 and 0.2. In figure (a) and (c) where only a pair of LFV are nonzero, only within a band $\langle s_{T_2} \rangle$ and $\langle P_{T_1} s_{T_2} \rangle$ can be large. This is expected because when there is a hierarchy between the nonzero elements, we expect a hierarchy between K_L and K_R as well as between A_L and A_R thus $\langle s_{T_2} \rangle$ and $\langle P_{T_1} s_{T_2} \rangle$ are suppressed. In figures (b) and (d), $(m_L^2)_{e\mu}$, $(m_R^2)_{e\mu}$, $(m_{LR}^2)_{e\mu}$ and $(m_{LR}^2)_{\mu e}$ are all nonzero. Notice that depending on the configuration of the LFV elements, the regions over which $\langle s_{T_2} \rangle$ and $\langle P_{T_1} s_{T_2} \rangle$ are large can have partial (like figures (a) and (d)) or complete (like figures (b) and (c)). This confirms our observation regarding the previous figures. In the case of overlap, one can

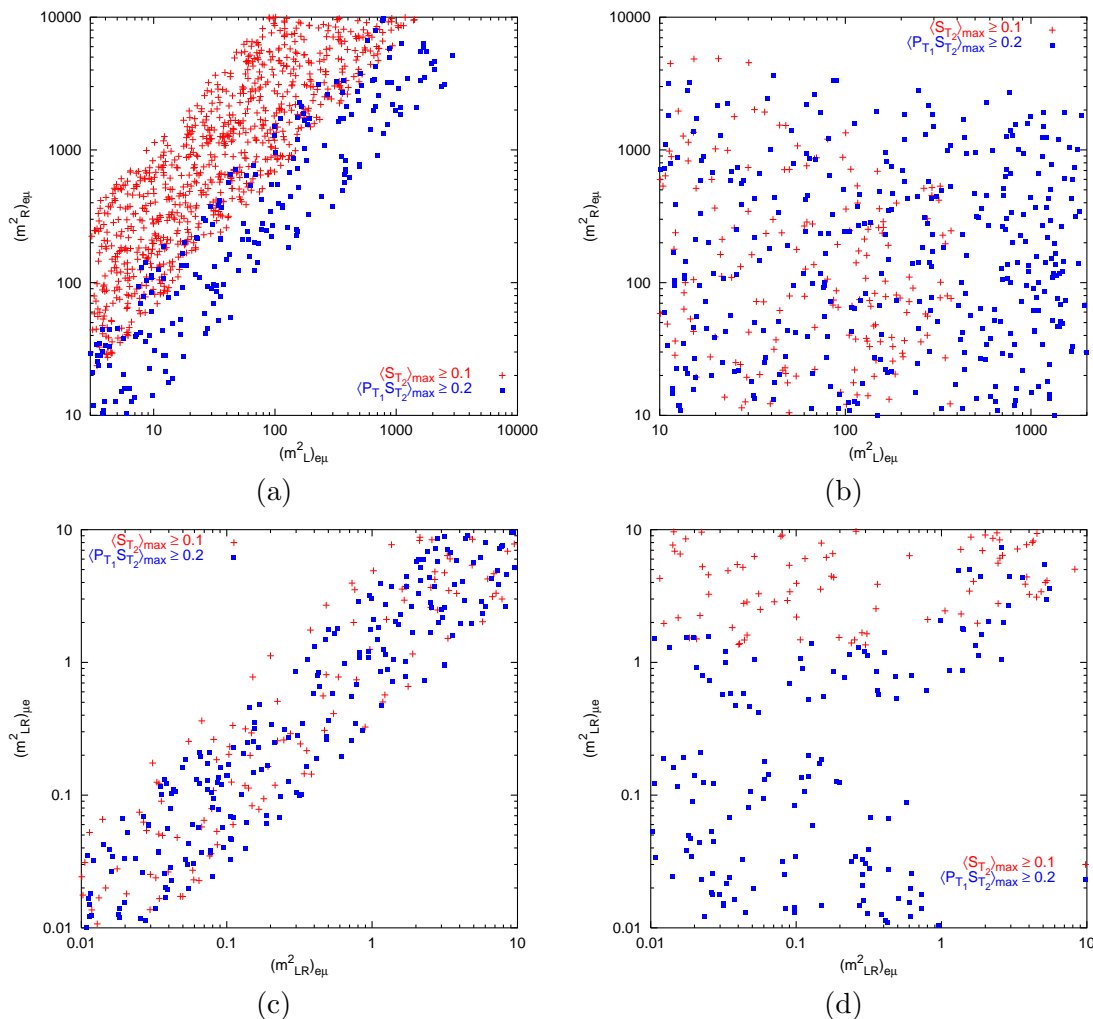


Figure 7: Scatter plots showing points for which $\overline{\langle s_{T_2} \rangle}$ at the $\mu N \rightarrow eN$ experiment with $\mathbb{P}_\mu = 20\%$ and $\overline{\langle P_{T_1} s_{T_2} \rangle}$ at the $\mu \rightarrow e\gamma$ experiment with $\mathbb{P}_\mu = 100\%$ are sizeable. The points depicted by plus (square) show the points at which the maximum value of $\overline{\langle s_{T_2} \rangle}$ ($\overline{\langle P_{T_1} s_{T_2} \rangle}$) is larger than 0.1 (0.2). The input for LF conserving parameters are the same as the input in figure 1: i.e., the P3 benchmark with $A_\mu = A_e = 700 \text{ GeV}$. In figure (a) all the LFV elements of the slepton mass matrix are set to zero except $(m^2_L)_{e\mu}$ and $(m^2_R)_{e\mu}$ which are randomly chosen respectively from $(3 \text{ GeV}^2, 3 \times 10^3 \text{ GeV}^2)$ and $(10 \text{ GeV}^2, 10^4 \text{ GeV}^2)$ at a logarithmic scale. The maximum polarization correspond to $\arg[(m^2_L)_{e\mu}] = \pi/2$ and $\arg[(m^2_R)_{e\mu}] = 0$. Figure (b) is similar to figure (a) except that $(m^2_{LR})_{e\mu} = (m^2_{LR})_{\mu e} = 4 \text{ GeV}^2$ and $(m^2_L)_{e\mu}$ and $(m^2_R)_{e\mu}$ are chosen respectively from $(2 \text{ GeV}^2, 2 \times 10^3 \text{ GeV}^2)$ and $(5 \text{ GeV}^2, 5 \times 10^3 \text{ GeV}^2)$. In figure (c), we have set $(m^2_L)_{e\mu} = (m^2_R)_{\mu e} = 0$ and allowed $(m^2_{LR})_{e\mu}$ and $(m^2_{LR})_{\mu e}$ to pick up random values at a logarithmic scale from the interval $(0.01 \text{ GeV}^2, 10 \text{ GeV}^2)$. In figure (d), we have set $(m^2_L)_{e\mu} = 100 \text{ GeV}^2$, $(m^2_R)_{e\mu} = 400 \text{ GeV}^2$ and allowed $(m^2_{LR})_{e\mu}$ and $(m^2_{LR})_{\mu e}$ to pick up random values from the interval $(0.01 \text{ GeV}^2, 10 \text{ GeV}^2)$.

employ both experiments to derive information on the CP-violating phases. In the next section, we discuss how by combining the information from these two experiments, one can derive extra information and resolve degeneracies.

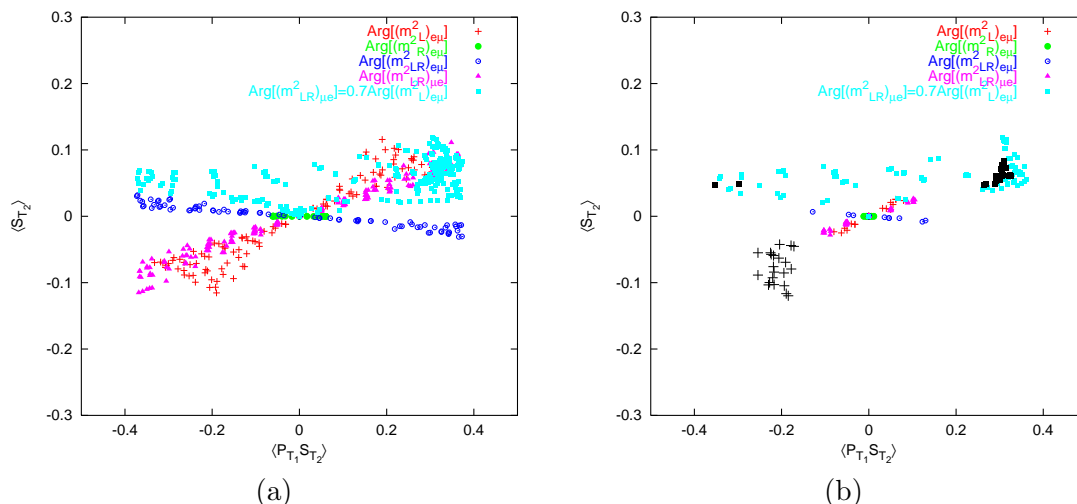


Figure 8: Transverse polarization in the $\mu \rightarrow e\gamma$ and $\mu\text{Ti} \rightarrow e\text{Ti}$ processes. The input for LF conserving parameters are the same as the input in figure 1: i.e., the P3 benchmark with $A_\mu = A_e = 700$ GeV. The only sources of LFV are the $e\mu$ elements. In calculating $\overline{\langle P_{T_1} s_{T_2} \rangle}$ (see eq. (2.10)) and $\overline{\langle s_{T_2} \rangle}$ (see eq. (3.10)) we have respectively set $\mathbb{P}_\mu = 100\%$ and $\mathbb{P}_\mu = 20\%$. Points depicted by various colors and symbols as described in the legend correspond to the case that the phases of various elements vary between 0 and 2π . The points show the correlation of $\overline{\langle P_{T_1} s_{T_2} \rangle}$ and $\overline{\langle s_{T_2} \rangle}$ at configurations of LFV for which $0.3 \leq R_1 \leq 0.4$, $0.7 \leq R_2 \leq 0.9$, $5.9 \times 10^{-12} \leq \text{Br}(\mu \rightarrow e\gamma) \leq 6.5 \times 10^{-12}$ and $8.5 \times 10^{-14} \leq R(\mu\text{Ti} \rightarrow e\text{Ti}) \leq 1.1 \times 10^{-13}$. In collecting the colored points in figure (b) we have removed the points for which $|d_e|$ exceeds 10^{-29} e cm (the reach of running experiments [24]). The black points in figure (b) depicted by slightly larger plus and squares satisfy the condition 2×10^{-29} e cm $< d_e < 3 \times 10^{-29}$ e cm.

5. Resolving degeneracies

As discussed in the previous sections, all the observables in the $\mu \rightarrow e\gamma$ experiment are determined by a pair of effective couplings (A_L, A_R) which in turn receive contributions from various parameters in the underlying theory. By measuring $\text{Br}(\mu \rightarrow e\gamma)$, R_1 and either of $\overline{\langle P_{T_1} s_{T_1} \rangle}$ and $\overline{\langle P_{T_1} s_{T_2} \rangle}$ (see, eqs. (2.9), (2.10)), one can reconstruct both A_L and A_R (up to a common phase). However, because of the degeneracies, it is not possible to unambiguously derive the values of the LFV elements and the CP-violating phases of the underlying theory from A_L and A_R .

Similarly to the $\mu \rightarrow e\gamma$ experiment, the observable quantities in the $\mu N \rightarrow eN$ experiment are given by a pair of parameters (K_L, K_R) which depend on the LFV masses and CP-violating phases of the underlying theory. By measuring $R(\mu N \rightarrow eN)$, R_2 and either of $\overline{\langle s_{T_1} \rangle}$ and $\overline{\langle s_{T_2} \rangle}$ (see, eqs. (3.9), (3.10)), it is possible to reconstruct $|K_L|$, $|K_R|$ and their relative phase; however, deriving the LFV and CP-violating parameters of the underlying theory from (K_L, K_R) would suffer from degeneracies.

Fortunately, the pairs of (K_L, K_R) and (A_L, A_R) depend on different combinations of the LFV elements. Thus, there is a hope to solve a part of degeneracies by combining information from the $(\mu \rightarrow e\gamma)$ and $(\mu N \rightarrow eN)$ experiments. Figure 8 demonstrates such

a possibility. In the case of the points depicted by red plus (+), green filled circle, dark blue circle and purple triangle, all the phases are set to zero except one of the phases which is specified in the legend and varies between 0 and 2π . In the case of points depicted by cyan squares, the phase of $(m_{LR}^2)_{\mu e}$ is set equal to 0.7 of the phase of $(m_L^2)_{e\mu}$ which varies between zero and $2\pi/0.7$ (thus, $\arg[(m_{LR}^2)_{\mu e}]$ varies between zero and 2π). The rest of the phases are set equal to zero. As we saw in the previous section, the sensitivity to the phase of A_μ is low (especially at the P3 benchmark) so in this analysis we have not considered this phase and focused on the effects of the phases of the LFV elements.

Hopefully, LHC will discover supersymmetry and provide us with information on the values of LF conserving parameters such as values of $\tan\beta$ and the masses of neutralinos, charginos (hence the values of M_2 and μ) and sfermions and etc. In the literature, it is discussed that under certain circumstances, LHC can also measure the LFV parameters [23]. However, in this analysis, we solely rely on the LFV rare processes $\mu \rightarrow e\gamma$ and $\mu N \rightarrow eN$ to derive the LFV parameters. Having this prospect in mind, we have chosen the values at the P3 benchmark for the lepton flavor conserving parameters. We have then searched for the values of the LFV $e\mu$ elements at which the observable quantities $\text{Br}(\mu \rightarrow e\gamma)$, $R(\mu\text{Ti} \rightarrow e\text{Ti})$, R_1 and R_2 are in a given range. We have fixed A_e and A_μ to 700 GeV. Notice that measuring $|A_\mu|$ and $|A_e|$ at LHC is going to be challenging if possible at all. In principle, we should have set A_μ and A_e as free parameters to be determined from the $\mu \rightarrow e\gamma$ and $\mu - e$ conversion experiments along with the LFV parameters. Notice however that, for $\tan\beta \gtrsim 10$, sensitivity to these parameters is low (i.e., varying A_i from 0 to 700 GeV, the changes in the values of the observables are less than 5%). If $\tan\beta$ turns out to be lower or a precision better than 5% is achieved, A_μ and A_e should be treated as free parameters (rather than input).

The idea behind the plot is as follows. Suppose $\mu \rightarrow e\gamma$ and $\mu\text{Ti} \rightarrow e\text{Ti}$ are detected and their rates are measured with some reasonable accuracy. Moreover suppose R_1 and R_2 are measured and found to be in the range indicated in the caption of figure 8. The question is what configurations of LFV elements and the CP-violating phases can give rise to these values of the observables. To answer this question, we have looked for the solutions by varying $|(m_L^2)_{e\mu}|$, $|(m_R^2)_{e\mu}|$, $|(m_{LR}^2)_{e\mu}|$ and $|(m_{LR}^2)_{\mu e}|$ respectively in the range (0, 10000) GeV², (0, 15000) GeV², (0, 50) GeV² and (0, 50) GeV² for given values of the CP-violating phases. We have then inserted the values of the LFV elements at the solutions in the formulas of $\overline{\langle s_{T_2} \rangle}$ and $\overline{\langle P_{T_1} s_{T_2} \rangle}$ and depicted it in figure 8a by a point.

From figure 8a, we observe that all sets of the solutions depicted with various symbols reach to each other at the point $\overline{\langle s_{T_2} \rangle} = \overline{\langle P_{T_1} s_{T_2} \rangle} = 0$. This is expected because setting the phases equal to zero renders A_L , A_R , K_L and K_R real so both $\overline{\langle s_{T_2} \rangle}$ and $\overline{\langle P_{T_1} s_{T_2} \rangle}$ vanish (see, eqs. (2.10), (3.10)). Apart from this point, the set of points depicted by plus and triangles are separate from points depicted by empty circles which means by combining information from the $\mu \rightarrow e\gamma$ and $\mu - e$ conversion searches, one can solve the degeneracy between these solutions. For example, if $|\overline{\langle s_{T_2} \rangle}| < 0.05$ and $\overline{\langle P_{T_1} s_{T_2} \rangle} \simeq 0.38$, we can make sure that neither of the solutions with zero $\arg[(m_{LR}^2)_{e\mu}]$ that we have considered in this analysis can be the case. However, the degeneracy is not completely solved. For example from figure 8a, we observe that the regions over which points depicted by plus and square are scattered,

overlap. At the intersection of the two regions, both $(\arg[(m_{LR}^2)_{\mu e}] = 0.7 \arg[(m_L^2)_{e\mu}] \neq 0)$ and $(\arg[(m_{LR}^2)_{\mu e}] = 0, \arg[(m_L^2)_{e\mu}] \neq 0)$ can be a solution.

We have repeated the same analysis for other ranges of $R_1, R_2, \text{Br}(\mu \rightarrow e\gamma)$ and $R(\mu\text{Ti} \rightarrow e\text{Ti})$. As long as R_1 and R_2 deviate from ± 1 , the above results are maintained. However, when R_1 and R_2 approach ± 1 , regardless of the values of the phases, the corresponding transverse polarizations become so small that in practice cannot be measured.

In summary, combining the information from $\mu \rightarrow e\gamma$ and $\mu N \rightarrow eN$ searches considerably lifts the degeneracies however, does not completely resolve them. By employing other observables, it may be possible to completely solve the degeneracies. For example, it is in principle possible to derive extra information on the $e\mu$ elements by studying other LFV processes such as $\mu \rightarrow e\gamma\gamma$ which within our scenario takes place with a rate suppressed by a factor of $O(e^2/16\pi^2)$ relative to the rate of $\mu \rightarrow e\gamma$. A more promising approach is to employ the information from the d_e searches. As we discussed in the previous section, the phases of the $e\mu$ elements can lead to $|d_e| \sim 10^{-29} e \text{ cm}$ which is within the reach of the currently running experiments [24]. To examine how much forthcoming results on d_e can help us to resolve the degeneracies, we have presented figure 8b. This figure is similar to figure 8a with the difference that at each point in addition to observables in the $\mu \rightarrow e\gamma$ and $\mu - e$ conversion experiments, we have also calculated d_e . We have removed the points for which $|d_e| > 10^{-29} e \text{ cm}$ from the set of points depicted by colored symbols. In the case of $(\arg[(m_{LR}^2)_{e\mu}] = 0, \arg[(m_L^2)_{e\mu}] \neq 0)$ and $(\arg[(m_{LR}^2)_{e\mu}] = 0.7 \arg[(m_L^2)_{e\mu}] \neq 0)$, we have also depicted points satisfying the condition $2 \times 10^{-29} e \text{ cm} < d_e < 3 \times 10^{-29} e \text{ cm}$ with slightly larger black symbols.

Notice that unlike in figure (a), in figure (b) the regions over which the squares and pluses are scattered have no overlap. This means d_e can help us to resolve the degeneracies. For example according to figures 8a,8b, if $\langle s_{T_2} \rangle$ and $\langle P_{T_1} s_{T_2} \rangle$ are measured and found to be respectively equal to 0.05 and 0.3, both $(\arg[(m_L^2)_{e\mu}] = 0, \arg[(m_{LR}^2)_{\mu e}] \neq 0)$ and $(\arg[(m_{LR}^2)_{\mu e}] = 0.7 \arg[(m_L^2)_{e\mu}] \neq 0)$ can be a solution. But if d_e turns out to be in the range $(2 - 3) \times 10^{-29} e \text{ cm}$, the solution with $(\arg[(m_L^2)_{e\mu}] = 0)$ will be excluded.

6. Conclusions

In this paper, we have first derived the formulas for the transverse polarization of the final particles in $\mu \rightarrow e\gamma, \mu \rightarrow eee$ and $\mu - e$ conversion in terms of the couplings of the effective LFV Lagrangian describing these processes. We have shown that by measuring these polarizations, one can derive information on the CP-violating phases of the underlying theory. We have then focused on the polarizations of the final particles in the $\mu \rightarrow e\gamma$ and $\mu - e$ conversion processes. We have found that for the configurations of LFV elements that asymmetries R_1 and R_2 (see eqs. (2.3), (3.6) for definitions) are not close to ± 1 , the transverse polarization can be sizeable and sensitive to certain combinations of the CP-violating phases. We therefore suggest the following steps as the strategy to extract the CP-violating phases. If in the future $\mu \rightarrow e\gamma$ and/or $\mu - e$ conversion is detected with high statistics, it will be possible to measure R_1 and/or R_2 by studying the angular distribution of the final particles relative to the spin of the decaying muon. If R_1 and/or R_2 turn

out to considerably deviate from ± 1 , it is then recommendable to equip the experiment with polarimeters to measure the transverse polarizations of the final particles and derive information on the phases of the effective couplings.

The above results apply to a general beyond SM scenario that provides large enough sources of LFV to allow detectable rates for $\mu \rightarrow e\gamma$ and $\mu N \rightarrow eN$. Within a given scenario, the couplings of the effective Lagrangian can depend on various parameters in the underlying theory. This leads to degeneracies in deriving these parameters. In this paper, we have addressed this problem in the context of R -parity conserving MSSM. We have implicitly assumed that supersymmetry would be discovered at the LHC and the lepton flavor conserving parameters relevant for this study (e.g., chargino and neutralino masses, slepton and sfermion masses and etc.) would be measured. We have then studied what can be learnt about the LFV and CP-violating parameters of MSSM at $\mu \rightarrow e\gamma$ and $\mu - e$ conversion experiments.

We have found that the dependence of the polarizations in the cases of $\mu \rightarrow e\gamma$ and $\mu - e$ conversion on the parameters of the underlying theory is different. As a result, depending on the configuration of the LFV elements, the effect can be sizeable in none, only one or both of the $\mu \rightarrow e\gamma$ and $\mu - e$ conversion processes. Thus, the polarization studies in these processes are complementary.

We have focused on the effect of the $e\mu$ elements and studied the dependence of the various observables on the phases of A_μ and the $e\mu$ LFV elements. Since there are already strong bounds on the phases of μ , M_1 (Bino mass) and A_e from electric dipole moment searches, we have taken these parameters real. We have found that for most parts of the parameter space with large $\tan\beta$ (i.e., $\tan\beta \sim 10$) the sensitivity to A_μ is low but the sensitivity of transverse polarizations both in $\mu \rightarrow e\gamma$ and $\mu - e$ conversion to $\arg[(m_L^2)_{e\mu}]$ is high. However, there are regions in the parameter space that the sensitivity to $\arg[A_\mu]$ is sizeable (e.g., the δ benchmark [22]). The sensitivity to $\arg[(m_R^2)_{e\mu}]$ in the case of $\mu \rightarrow e\gamma$ is also high but in the case of the $\mu - e$ conversion, the sensitivity to $\arg[(m_R^2)_{e\mu}]$ is low.

In the context of the present scenario, various CP-violating parameters can affect the observables in the $\mu \rightarrow e\gamma$ and $\mu N \rightarrow eN$ experiments. These polarizations also strongly depend on the ratios of the absolute values of the various LFV elements. We have shown that for configurations of LFV elements for which $-0.9 < R_1, R_2 < 0.9$, combining information on $R_1, R_2, \text{Br}(\mu \rightarrow e\gamma)$ and $R(\mu N \rightarrow eN)$ with information on the transverse polarization of the final particles can help us to considerably decrease degeneracies and derive information on these phases. However, information from these measurements is not enough to fully resolve degeneracies. For example, we have shown degeneracies between solutions ($\arg[(m_{LR}^2)_{\mu e}] = 0, \arg[(m_L^2)_{e\mu}] \neq 0$) and ($\arg[(m_{LR}^2)_{\mu e}] = 0.7 \arg[(m_L^2)_{e\mu}] \neq 0$) cannot be removed even when we use all the information accessible at the $\mu \rightarrow e\gamma$ and $\mu N \rightarrow eN$ search experiments. To fully resolve the degeneracies, extra information from other experiments has to be employed. We have also demonstrated that the forthcoming results of the d_e search can help us to remove the degeneracies further.

Notice that by [simultaneously] turning on the $\mu\tau$ and $e\tau$ elements, more degeneracies will emerge. To resolve these degeneracies, one can employ other observables such as $\text{Br}(\tau \rightarrow e\gamma)$ and $\text{Br}(\tau \rightarrow \mu\gamma)$. Studying the general case is beyond the scope of the present

paper and will be presented elsewhere.

We have also briefly discussed the possibility to derive further information by using different nuclei in the $\mu - e$ conversion experiment and found that since the ratio of proton number to the neutron number for different nuclei is close to each other, the polarizations are similar for different nuclei. Unless a precision better than 5% is achieved, changing the nuclei will not help us to extract information on an extra combination of the parameters but can be considered as a cross-check of the results.

Acknowledgments

We would like to thank M. M. Sheikh-Jabbari for careful reading of the manuscript and the useful remarks.

References

- [1] S.T. Petcov, *The processes $\mu \rightarrow e\Gamma$, $\mu \rightarrow ee\bar{e}$, neutrino' \rightarrow neutrino γ in the Weinberg-Salam model with neutrino mixing*, *Sov. J. Nucl. Phys.* **25** (1977) 340 [*Yad. Fiz.* **25** (1977) 641] [*Erratum ibid.* **25** (1977) 698] [*Erratum ibid.* **25** (1977) 1336];
S.M. Bilenky, S.T. Petcov and B. Pontecorvo, *Lepton mixing, $\mu \rightarrow e + \gamma$ decay and neutrino oscillations*, *Phys. Lett.* **B 67** (1977) 309;
G. Altarelli, L. Baulieu, N. Cabibbo, L. Maiani and R. Petronzio, *Muon number nonconserving processes in gauge theories of weak interactions*, *Nucl. Phys.* **B 125** (1977) 285 [*Erratum ibid.* **130** (1977) 516].
- [2] PARTICLE DATA GROUP collaboration, W.M. Yao et al., *Review of particle physics*, *J. Phys.* **G 33** (2006) 1.
- [3] <http://meg.web.psi.ch/index.html>;
see also MEG collaboration, M. Grassi, *The MEG experiment at PSI: status and prospect*, *Nucl. Phys.* **149** (*Proc. Suppl.*) (2005) 369.
- [4] Y. Kuno and Y. Okada, *Muon decay and physics beyond the standard model*, *Rev. Mod. Phys.* **73** (2001) 151 [[hep-ph/9909265](#)];
J.L. Feng, *Theoretical motivations for lepton flavor violation*, [hep-ph/0101122](#).
- [5] Y. Farzan, *Tracing CP-violation in lepton flavor violating muon decays*, *JHEP* **07** (2007) 054 [[hep-ph/0701106](#)].
- [6] R.M. Godbole, *CP violation in supersymmetry and the LHC*, *Czech. J. Phys.* **55** (2005) B221 [[hep-ph/0503088](#)];
O. Kittel, *CP violation in production and decay of supersymmetric particles*, [hep-ph/0504183](#);
S. Heinemeyer and M. Velasco, *Exploring complex phases of the MSSM at future colliders*, in the proceedings of the 2005 *International Linear Collider Workshop (LCWS2005)*, March 18–22, Stanford, California, U.S.A. (2005), [hep-ph/0506267](#).
- [7] A. van der Schaaf, *SINDRUM II*, *J. Phys.* **G 29** (2003) 1503;
SINDRUM II collaboration, W. Bertl et al., *A search for $\mu - e$ conversion in muonic gold*, *Eur. Phys. J.* **C 47** (2006) 337.

- [8] P. Wintz, *Results of the SINDRUM-II experiment*, in *Proceedings of the First International Symposium on Lepton and Baryon number Violation*, H.V. Kalpdor-Kleingrothaus and I.V. Krivosheina eds., Institute of Physics Publishing, U.K. (1998).
- [9] M. Aoki, *PRISM: experiment*, prepared for the *Joint U.S./Japan Workshop on New Initiatives in Muon Lepton Flavor Violation and Neutrino Oscillation with High Intense Muon and Neutrino Sources*, October 2–6, Honolulu, Hawaii, U.S.A. (2000);
 Y. Mori, *PRISM: a phase rotator to obtain an intense monochromatic muon beam*, prepared for the 7th *European Particle Accelerator Conference (EPAC2000)*, June 26–30, Vienna, Austria (2000);
 Y. Kuno, *PRISM/PRIME*, *Nucl. Phys.* **149** (Proc. Suppl.) (2005) 376;
 see also, E.J. Prebys et al., *Expression of interest: a muon to electron conversion experiment at Fermilab*, FERMILAB-TM-2389-AD-E.
- [10] S. Davidson, *CP violating phases in $\mu - e$ conversion*, [arXiv:0809.0263](https://arxiv.org/abs/0809.0263).
- [11] J. Hisano, T. Moroi, K. Tobe and M. Yamaguchi, *Lepton-flavor violation via right-handed neutrino Yukawa couplings in supersymmetric standard model*, *Phys. Rev.* **D 53** (1996) 2442 [[hep-ph/9510309](https://arxiv.org/abs/hep-ph/9510309)].
- [12] Y. Okada, K.-I. Okumura and Y. Shimizu, *$\mu \rightarrow e\gamma$ and $\mu \rightarrow 3e$ processes with polarized muons and supersymmetric grand unified theories*, *Phys. Rev.* **D 61** (2000) 094001 [[hep-ph/9906446](https://arxiv.org/abs/hep-ph/9906446)].
- [13] H. Burkard et al., *Muon decay: measurement of the transverse positron polarization and general analysis*, *Phys. Lett.* **B 160** (1985) 343.
- [14] P.F. Bloser, S.D. Hunter, G.O. Depaola and F. Longo, *A concept for a high-energy gamma-ray polarimeter*, [astro-ph/0308331](https://arxiv.org/abs/astro-ph/0308331);
 F. Adamyan et. al, *A photon beam polarimeter based on nuclear $e+e-$ pair production in an amorphous target*, *Nucl. Instrum. Meth.* **A546** (2005) 376.
- [15] V.S. Evseev, *Muon physics. Vol. III: chemistry and solids*, V.W. Hughes and C.S. Wu eds., Academic Press, U.S.A. (1975), p. 236.
- [16] K. Nagamine and T. Yamazaki, *Polarized muonic atoms*, *Nucl. Phys.* **A 219** (1974) 104;
 Y. Kuno, K. Nagamine and T. Yamazaki, *Polarization transfer from polarized nuclear spin to $\mu-$ spin in muonic atom*, *Nucl. Phys.* **A 475** (1987) 615.
- [17] S. Yaser Ayazi and Y. Farzan, *Reconciling large CP-violating phases with bounds on the electric dipole moments in the MSSM*, *Phys. Rev.* **D 74** (2006) 055008 [[hep-ph/0605272](https://arxiv.org/abs/hep-ph/0605272)], and references therein.
- [18] S.Y. Ayazi and Y. Farzan, *Electron electric dipole moment from lepton flavor violation*, *JHEP* **06** (2007) 013 [[hep-ph/0702149](https://arxiv.org/abs/hep-ph/0702149)].
- [19] A. Bartl, W. Majerotto, W. Porod and D. Wyler, *Effect of supersymmetric phases on lepton dipole moments and rare lepton decays*, *Phys. Rev.* **D 68** (2003) 053005 [[hep-ph/0306050](https://arxiv.org/abs/hep-ph/0306050)];
 W. Porod, *Effect of supersymmetric phases on lepton dipole moments and rare lepton decays*, prepared for the *International Workshop on Astroparticle and High-Energy Physics (AHEP – 2003)*, October 14–18, Valencia, Spain (2003).
- [20] J. Ellis, T. Hahn, S. Heinemeyer, K.A. Olive and G. Weiglein, *WMAP-compliant benchmark surfaces for MSSM Higgs bosons*, *JHEP* **10** (2007) 092 [[arXiv:0709.0098](https://arxiv.org/abs/hep-ph/0709.0098)];
 S. Heinemeyer, *Higgs-boson benchmarks in agreement with CDM, EWPO and BPO*, [arXiv:0710.3014](https://arxiv.org/abs/hep-ph/0710.3014).

- [21] J.A. Casas and S. Dimopoulos, *Stability bounds on flavor-violating trilinear soft terms in the MSSM*, *Phys. Lett. B* **387** (1996) 107 [[hep-ph/9606237](#)].
- [22] A. De Roeck et al., *Supersymmetric benchmarks with non-universal scalar masses or gravitino dark matter*, *Eur. Phys. J. C* **49** (2007) 1041 [[hep-ph/0508198](#)].
- [23] J.L. Diaz-Cruz, D.K. Ghosh and S. Moretti, *Lepton flavour violating heavy Higgs decays within the nuMSSM and their detection at the LHC*, [arXiv:0809.5158](#).
- [24] D. DeMille et al., *Search for the electron electric dipole moment*, *AIP Conf. Proc.* **842** (2006) 759.